The Rosetta Mars Flyby

Niklas Edberg

21st February 2006

We focus on a short, but interesting, episode of the decade-long Rosetta mission. In February 2007 the Rosetta spacecraft will pass by the planet Mars. The Langmuir probes onboard, provided by the Swedish Institute of Space Physics, Uppsala, have the rare opportunity of measuring features of the Martian plasma environment and careful planning is therefore needed.

We investigate the trajectory of Rosetta during the flyby by further development of Matlab routines for reading in data, transforming between coordinate systems and plotting of the trajectory.

A literature study and summary of the Martian plasma environment, and models of it, is conducted before we implement an existing model ourselves. We use the results of a three-dimensional multi-species hybrid simulation and obtain global maps of the plasma parameter values around Mars as well as expected time series of what Rosetta will measure during the flyby. We find that Rosetta will pass through all the major plasma boundaries and regions.

Additionally, we use a model of the crustal magnetic field of Mars and obtain global maps of the magnetic field and expected time series of the magnetic field which Rosetta will encounter.

We also look at some further upcoming events, such as the Earth flybys in 2007 and 2009 and possible conjunctions between Rosetta and Mars along the magnetic field from the Sun.

Sammanfattning

Detta arbete har gjorts som en förberedelse inför rymdfarkosten Rosettas förbiflygning av planeten Mars. Rosettas huvudsakliga mål är att komma ifatt en komet, lägga sig i omloppsbana runt den och göra detaljerade studier av kometens egenskaper, som till exempel sammansättning, växelverkan med solvinden m.m. Ombord på Rosetta finns också en landare som är tänkt att släppas ner till kometkroppen och utföra ännu mer detaljerade studier. För att komma ifatt kometen, som har en hastighet på flera tiotals kilometer per sekund, måste Rosetta accelereras. Detta sker genom planetförbiflygningar då planetens gravitation ger den extra skjuts som behövs. Rosetta sköts upp år 2004 och kometen är planerad att nås 2014. Under dessa tio år kommer fyra planetförbiflygningar att äga rum, jorden ska passeras tre gånger och Mars en gång.

Den 25:e februari 2007, klockan 01:55 UT, kommer Rosetta att vara som allra närmast Mars med en höjd på omkring 250 km, vilket är långt nere i Mars jonosfär (det översta, joniserade lagret av atmosfären). Detta är ett utmärkt tillfälle för mätningar av plasmat i Mars omgivningen och för att få ut det mesta av mätningarna är det viktigt med noggranna förberedelser. Institutet för Rymdfysik i Uppsala är ansvariga för ett av de vetenskapliga instrumenten ombord - Langmuirprober. Detta instrument kan liknas vid en väderstation för rymdplasma och kan mäta temperaturer, flödeshastigheter och tätheter.

Vi har i detta arbete vidareutvecklat och skrivit nya Matlab-program för att läsa in bandata och göra koordinattransformationer mellan olika koordinatsystem och på så sätt visualisera Rosettas bana. Att ha banan ritade i olika koordinatsystem ger en god överblick av geometrin vid förbiflygningen och det blir lättare att se genom vilka områdeen farkosten kommer att åka.

Egenskaperna för Mars plasmaomgivning styrs av hur solvinden, en vind av elektriskt laddad gas (plasma) som ständigt blåser ut från solen, växelverkar med planeten. För Mars sker växelverkan direkt med den yttre atmosfären runt planeten och inte med ett globalt magnetfält som för jorden. Vi har implementerat en tredimensionell modell för denna växelverkan och jämfört modellens värden på plasmaparametrarna med Rosettas bana. Detta har gett oss tidsserier av vad Rosetta kan komma att mäta upp under dess förbiflygning.

Mars har inget globalt magnetfält, liknande det vi har på jorden. Det finns dock ett magnetfält med ursprung i Mars-skorpan. Innan Mars stelnade långt tillbaka i tiden,

magnetiserades skorpan av det då existerande inre magnetfälet. När kärnan sedan stelnade försvann det inre magnetfältet medan magnetiseringen av skorpan bestod. Denna magnetisering är dock mycket ojämn i styrka och i var det befinner sig - det är huvudsakligen det södra halvklotet som är magnetiserat. Vi har implementerat en modell av detta magnetfält och jämfört med Rosettas bana för att, på samma sätt som ovan, få ut en tidsserie av vad Rosetta kan komma att mäta upp.

Vi undersöker även möjligheterna för att kunna göra solvindsmätningar längs så kallade Parkerspiraler mellan Rosetta och Mars. Detta är av intresse för andra satelliter runt Mars som undersöker plasmaomgivningen. Längs en Parkerspiral-linje förändras solvinden, och däri det infrusna interplanetära magnetfältet, på ett enkelt och förutsäbart sätt. Detta innebär att man vet hur det interplanetära magnetfältet såg ut innan det träffade Mars, vilket i sin tur kan jämföras med mätningar runt Mars, för att på så sätt få reda på hur växelverkan med Mars fungerar.

Contents

Chapter 1

Introduction

In February 2007 the Rosetta spacecraft, one of the cornerstone missions of the European Space Agency (ESA), will fly by the planet Mars. In order to make the most out of this rare opportunity, careful planning is needed. The closest approach will be about 250 km and the entire flyby will last for approximately 45 minutes (below an altitude of 10 000 km from the surface of Mars). Rosetta will pass well within the plasma environment of Mars and therefore many interesting features can be measured with the plasma instruments onboard. The Rosetta spacecraft is built by Astrium for ESA while the payload, i.e. all the scientific instruments, is a collaboration between numerous institutes, universities and research groups all over Europe. The final objective with Rosetta is to catch up with the comet 67P/Churyumov-Gerasimenko in 2014. The Swedish Institute of Space Physics in Uppsala (IRFU) has provided one of the instruments onboard, using two identical, so called Langmuir probes. This instrument is used for measuring basic parameters of the space plasma, such as temperature, density, flow velocity and electric fields.

Figure 1.1: An artists view of the Rosetta spacecraft approaching Mars. Image from ESA.

This thesis is three-fold, meaning that we mainly focus on three subjects - the trajectory of Rosetta, the plasma environment around Mars and the crustal magnetic field on Mars. The outline of the thesis is stated below.

In Chapter 2 the trajectory of Rosetta is identified and plotted in some useful ways in order to show which parts of the plasma environment Rosetta will encounter. This is done by further development of already existing Matlab routines for reading in trajectory data and transforming between different coordinate systems and trajectory plotting.

In Chapter 3 we describe what is already known about the plasma environment of Mars. A literature study is conducted and summarised. A global simulation of the solar wind interaction with Mars is also used in this chapter. The model gives a three dimensional description of the Martian ionized environment, providing, for instance, an estimation of the densities, temperatures and velocities for different ion species. It can also characterize the draping of the interplanetary magnetic field around the planet. We compare this model with the Rosetta trajectory in order to find out what Rosetta might encounter during the flyby.

In Chapter 4 we implement a model of the crustal magnetic field of Mars which allow us to map the magnetic field strength around Mars. The Rosetta trajectory is compared with this model as well.

In Chapter 5 we give a brief introduction to the Langmuir probes onboard Rosetta. The basic design and function is described.

In Chapter 6 we take a brief look at some further upcoming events for the Rosetta spacecraft, such as the second and third Earth-flybys and possible Parker spiral conjunctions before we conclude our work in Chapter 7.

1.1 Purpose

There are two main purposes for doing this preparatory work. First of all, exploring what is expected to be measured by Rosetta during the Mars flyby will give a good background for the decision on what measurement mode the scientific instruments onboard should be in, at least for the instruments used for plasma measurements. Secondly, predictions of the measured features will help in understanding the actual data later on. It will be easier to understand what the data shows if there is a solid background study.

There are some additional objectives as well. First, the trajectories of the next two Earth flybys are interesting to identify in order to get an idea of what is coming. Second, to find out if there will be any Parker spiral conjunctions with Rosetta and Mars would be very interesting for other spacecraft in operation at Mars. During the conjunction Rosetta could provide a rough estimation of the solar wind plasma parameters; essentially the magnetic field which influence the plasma environment close to the planet.

1.2 The Rosetta Mission

The Rosetta spacecraft was launched by an Ariane-5G+ rocket in early 2004 from Kourou, French Guiana, after many years of planning, designing and constructing. The launch was nothing but successful, setting the spacecraft "en route" to the comet 67P/Churyumov-Gerasimenko. The catching up with the comet will not take place until 2014, making the Rosetta mission into a quite long-lasting space exploration mission. One of the reasons for this long journey is the fact that the comet moves at a speed of several tens of kilometres per second. Rosetta of course needs to be accelerated to these velocities.

Acceleration of a spacecraft in this case is impossible to do by just bringing an enormous amount of fuel into space and igniting the engine. It requires too much energy to lift such an amount of fuel into space. Instead, acceleration is conducted by using the gravitational pull of other bodies - such as planets - during flybys. The principle of a flyby is to "steal" momentum from the other body by using its gravitation as a sling shot. As the spacecraft approaches the planet the gravitation will constantly cause an acceleration. The spacecraft will after the flyby have gained quite a lot of speed while the planet have lost a small fraction (due to the enormous difference in mass). Rosetta will make four such flybys: one flyby of the Earth has already been conducted in 2005, the next one will be the Mars flyby in 2007, and then there will be two more Earth flybys in late 2007 and 2009.

There will also be time for two asteroid passes in between these flybys so even though the journey to the comet will last for ten years, Rosetta will not be lonely during the trip. Table 1.1 shows the general outline of the entire mission.

Table 1.1: The Rosetta mission.

Date	Event
2 Mar 2004	Launch
4 Mar 2005	First Earth flyby
25 Feb 2007	**Mars flyby**
14 Nov 2007	Second Earth flyby
5 Sep 2008	Asteroid Steins passing
11 Nov 2009	Third Earth flyby
10 Jul 2010	Asteroid Lutetia passing
Aug 2014	Catch up with the comet
Nov 2014	Landing on the comet
Aug 2015	Perihelion

When the destination is reached in 2014, Rosetta will be set into orbit around the comet which in turn moves fast towards the Sun. It will take about one year for the comet to reach perihelion, i.e. the point in its path closest to the Sun, after Rosetta's encounter. During this time the comet, slowly melting and evaporating, will be intensively studied by the many different scientific instruments onboard Rosetta. There is also a lander,

named Philae, that will land on the surface of the comet.

Onboard Rosetta, which consists of a 2.8 x 2.1 x 2.0 metres large body and two 16 metre long solar panels, there are about ten different scientific instruments or groups of instruments. One of these groups is the Rosetta Plasma Consortium (RPC) out of which one type of instrument is built by IRFU.

1.3 Previous Missions to Mars

The Rosetta Mars flyby is a great opportunity for conducting plasma measurements at Mars. Only a few spacecraft have ever visted Mars and few of them have had such good plasma instruments onboard as Rosetta. Table 1.2 shows a list of previous spacecraft that have ever reached/attempted to reach the planet Mars. There have been quite many attempts, mainly conducted by USSR/Russia and the USA but in recent years even Japan and the European Space Agency (ESA) has tried to reach/reached the planet.

Out of 36 attempts to reach Mars, 16 were successful. Of these 16 missions only a handful had adequate plasma instruments onboard. The following list is a summary of those spacecraft that have had plasma instruments onboard and that actually performed measurements, and what type of instruments they carried for plasma measurements [NSSDC Master catalog, 2005].

Mariner 4 A Vector Low-field Helium Magnetometer was used to measure the interplanetary magnetic field up to 1 Hz.

A Cosmic-Ray Telescope was used to determine proton fluxes in the energy range 15 to 70 MeV and 70 to 170 MeV, alpha particles in the range 15 to 70 MeV/nucleon and above 70 MeV/nucleon, and protons and alpha particles in the energy interval 1.2 to 15 MeV.

Occultation experiments were used to infer properties of the Martian atmosphere by sending telemetry signals back to Earth through the atmosphere of Mars, which then changed intensity and phase depending on the properties of the atmosphere.

Mars 2 and Mars 3 Each S/C carried with them eight separate narrow angle electrostatic plasma sensors to determine speed, temperature and composition of the solar wind in the range 30 eV to 10000 eV, as well as a three axis magnetometer to measure the interplanetary and Martian magnetic field.

Mars 5 and Mars 6 Each S/C carried a magnetometer, plasma ion traps and a narrow angle electrostatic plasma sensor. They also conducted occultation experiments.

Viking 1 and 2 Carried radio science instruments on the orbiters and landers and also magnetic properties instruments and retarding potential analyzers on the landers. These instruments determined magnetic properties as well as physical and chemical properties of the atmosphere, such as structure, composition and temperature of the ionosphere.

Phobos 1 and 2 Together carried instruments to characterise the entire plasma environment around Mars, e.g. ASPERA for ion measurements. Energy, mass, and charge spectrometer, energetic charged-particle spectrometer, magnetometers, ion mass analyser, plasma wave systems, ion and electron spectrometer.

Mars Global Surveyor Carries a magnetometer and an electron reflectometer to determine the strength and orientation of the magnetic field.

Mars Express carries the ASPERA-3 instrument for ion, electron and neutral atom analysis.

Note that each of these spacecraft carried several other instruments but not all instruments could be used for plasma measurements.

Table 1.2: Previous missions to Mars. Those written in italics failed [The Planetary Society, 2005], [NSSDC Master catalog, 2005].

Spacecraft	Launch	Country	Mission	Closest App. (km)	Success
Korabl 4 (Marsnik 1)	*1960*	*USSR*	*Flyby*	-	No
Korabl 5 (Marsnik 2)	*1960*	*USSR*	*Flyby*	-	No
Korabl 11 (Sputnik 22)	*1962*	*USSR*	*Flyby*	-	No
Mars 1 (Sputnik 23)	*1962*	*USSR*	*Flyby*	-	No
Korabl 13 (Sputnik 24)	*1962*	*USSR*	*Lander*	-	No
Mariner 3	*1964*	*USA*	*Flyby*	-	No
Mariner 4	1964	USA	Flyby	9844	Yes
Zond 2	*1964*	*USSR*	*Flyby, Lander*	-	No
Mariner 6	1969	USA	Flyby	3431	Yes
Mariner 7	1969	USA	Flyby	3430	Yes
Mars 1969A	*1969*	*USSR*	*Orbiter*	-	No
Mars 1969B	*1969*	*USSR*	*Orbiter*	-	No
Mariner 8	*1971*	*USA*	*Flyby*	-	No
Kosmos 419	*1971*	*USSR*	*Orbiter*	-	No
Mars 2	1971	USSR	Orbiter, Lander	0	Yes
Mars 3	1971	USSR	Orbiter, Lander	0	Yes
Mariner 9	1971	USA	Orbiter	1398	Yes
Mars 4	*1973*	*USSR*	*Orbiter*	2200	No
Mars 5	1973	USSR	Orbiter	1755	Yes
Mars 6	1973	USSR	Flyby, Lander	0	Yes
Mars 7	*1973*	*USSR*	*Lander*	-	No
Viking 1	1975	USA	Orbiter, Lander	0	Yes
Viking 2	1975	USA	Orbiter, Lander	0	Yes
Phobos 1	*1988*	*USSR*	*Orbiter*	-	No
Phobos 2	1988	USSR	Orbiter, Landers	9080/-	Yes
Mars Observer	*1992*	*USA*	*Orbiter*	-	No
Mars Global Surveyor	1996	USA	Orbiter	171	Yes
Mars 96	*1996*	*Russia*	*Orbiter, lander*	-	No
Pathfinder	1996	USA	Lander, Rover	0	Yes
Nozomi (Planet B)	*1998*	*Japan*	*Orbiter*	-	No
Mars Climate Orbiter	*1998*	*USA*	*Orbiter*	-	No
Mars Polar Lander	*1999*	*USA*	*Lander*	-	No
Deep Space 2	*1999*	*USA*	*Penetrators*	-	No
2001 Mars Odyssey	2001	USA	Orbiter	400	Yes
Mars Express/*Beagle 2*	2003	ESA	Orbiter/*Lander*	259/-	Yes/No
Spirit/Opportunity	2003 -	USA	Rovers	0	Yes
Rosetta	**2004**	**ESA**	**Flyby**	**250**	**?**
Mars Reconnaissance Orb.	2005	USA	Orbiter	-	?

Chapter 2

The Rosetta Trajectory During the Mars Flyby

One important part of planning the Rosetta Mars Flyby is to read the trajectory data files, transform the coordinates into useful coordinate systems and plot the trajectory during the flight. The trajectory has of course been determined prior to the launch (even though small corrections and changes can take place post-launch). In order to plot the trajectory in a way that is useful for planning and evaluating measurements, Matlab routines for reading the data files and make trajectory plots have been developed by a former master thesis worker, Magnus Billvik [Billvik, 2005]. However, these routines where not complete for the Mars flyby and hence have been further developed in this thesis work. This chapter will describe how the data files are obtained and read, transformed and plotted by these Matlab routines.

2.1 Coordinate Systems and Transformations

The raw trajectory data files are provided by the European Space Operations Centre (ESOC) through their Data Distribution System (DDS) for the Rosetta spacecraft and by NASA Jet Propulsion Laboratory's HORIZONS System for all the celestial bodies (you actually send in an e-mail according to the instructions at the JPL site and get the data files in return [JPL's Horizons System, 2005]). The position coordinates for Rosetta, for the Mars flyby, are received in a Mars centred Earth-equatorial Inertial system (MEI), i.e. the centre is in Mars, the xy-plane is the Earth's equatorial plane, the positive x-axis points towards the vernal equinox of the Earth[1], the z-axis is directed along the Earth's spin axis and the y-axis completes the right-handed system. The position coordinates for the celestial bodies are given in a Geocentric Ecliptic Inertial system (GEA), i.e. the

[1]The vernal equinox is the point towards which the intersection line between the equatorial plane and the orbital plane points and as there are two such points, the vernal equinox is defined as the one point where the body moves from south to north. It is also called the first point of Aries (for the Earth).

xy-plane is the ecliptic plane[2], the positive x-axis points towards the vernal equinox of the Earth, the positive z-axis is directed to the ecliptic north and the y-axis completes the right-handed system.

These coordinates for the Rosetta spacecraft and the celestial bodies are then transformed into other coordinate systems by Matlab routines in order to get useful plots of the events around Mars. The coordinate systems which are used are tabulated below.

Table 2.1: Coordinate systems used for describing the Rosetta position coordinates into useful reference frames. A * indicates that the names are not commonly used but invented for these transformations.

Coordinate system	Centre	Direction of x-axis	Direction of z-axis
GEA (Geoc. Ecliptic Aries)	Earth	Earth vernal equinox	Ecliptic north
MEI (Marsc. Earth Equ. Inertial)*	Mars	Earth vernal equinox	Earth spin axis
MEA (Marsc. Ecliptic Aries)*	Mars	Earth vernal equinox	Ecliptic north
MEC (Marsc. Ecliptic Asc. node)*	Mars	Mars ascending node	Ecliptic north
MOC (Marsc. Orbital Asc. node)*	Mars	Mars ascending node	Normal to Mars orbital plane
MSO (Mars Solar Orbital)	Mars	Mars-Sun line	Normal to Mars orbital plane
MRX (Marsc. Equatorial Equinox)*	Mars	Mars vernal equinox	Mars spin axis
MEO (Areographical Cartesian)*	Mars	$Long = Lat = 0$	Mars spin axis
Areographical	Mars	$Long = 0$ at Airy-0 crater	$Latitude = 0$ at Mars equator

The two coordinate systems that are of primary interest to us are the Mars Solar Orbital system (MSO) and the Areographical system. The MSO coordinate system is useful because it has one axis always pointing towards the Sun which is of critical importance when dealing with space physics. The Areographical system (Mars geographical system) gives the longitude and latitude (and altitude) of a point. The MEO system and the Areographical system are actually the same system but in Cartesian and spherical representations.

The Matlab routines for transforming and translating between these systems are the following:

GEA to MEA gea2mea.m moves the centre of the reference frame from the Earth to Mars by subtracting the position of Rosetta in GEA-coordinates from the position of Mars in GEA-coordinates,

$$\begin{bmatrix} x_{\text{Rosetta}} \\ y_{\text{Rosetta}} \\ z_{\text{Rosetta}} \end{bmatrix}_{\text{MEA}} = \begin{bmatrix} x_{\text{Mars}} \\ y_{\text{Mars}} \\ z_{\text{Mars}} \end{bmatrix}_{\text{GEA}} - \begin{bmatrix} x_{\text{Rosetta}} \\ y_{\text{Rosetta}} \\ z_{\text{Rosetta}} \end{bmatrix}_{\text{GEA}} . \tag{2.1}$$

[2]The ecliptic plane is the plane in which the Earth orbits the Sun.

but the axis still points to Earth-relevant direction (i.e. first point of Aries)

MEI to MEA mei2mea.m turns the coordinate system around the x-axis until the z-axis has moved from the Earth's spin axis to the ecliptic north. This is done by multiplying the MEI-coordinates with the rotation matrix P, see Appendix A.1. The angle to rotate is equal to the Earth axial obliquity $o = 23.439291°$,

$$\begin{bmatrix} x \\ y \\ z \end{bmatrix}_{\text{MEA}} = \big[P(o)\big] \begin{bmatrix} x \\ y \\ z \end{bmatrix}_{\text{MEI}} . \tag{2.2}$$

MEA to MEC to MOC mea2moc.m first turns the coordinate system around the z-axis until the x-axis has moved from the Earth vernal equinox to the line of intersection between the ecliptic plane and Mars' orbital plane (Mars ascending node). This is done by multiplying the MEA-coordinates with the rotation matrix R. The angle to rotate is equal to longitude of Mars ascending node $\Omega = 49.57854°$,

$$\begin{bmatrix} x \\ y \\ z \end{bmatrix}_{\text{MEC}} = \big[R(\Omega)\big] \begin{bmatrix} x \\ y \\ z \end{bmatrix}_{\text{MEA}} . \tag{2.3}$$

The MEC coordinate system is then rotated around the x-axis until the z-axis has moved from the ecliptic north to the normal of Mars orbital plane. This is done by multiplying the MEC-coordinates with the rotation matrix P. The angle to rotate is equal to Mars' orbital inclination $i = 1.85°$,

$$\begin{bmatrix} x \\ y \\ z \end{bmatrix}_{\text{MOC}} = \big[P(i)\big] \begin{bmatrix} x \\ y \\ z \end{bmatrix}_{\text{MEC}} . \tag{2.4}$$

MOC to MSO moc2mso.m turns the coordinate system around the z-axis until the the x-axis has moved from the intersection line of the ecliptic and Mars' orbital plane to the direction of the Sun. This is done by multiplying the MOC-coordinates with the rotation matrix R. The angle to rotate, which changes as the Sun moves, is equal to the longitude of the Sun $l = \arctan(\frac{y_{\text{MOC}}(\text{Sun})}{x_{\text{MOC}}(\text{Sun})})$, i.e. the angle between Mars ascending node and the Sun,

$$\begin{bmatrix} x \\ y \\ z \end{bmatrix}_{\text{MSO}} = \big[R(l)\big] \begin{bmatrix} x \\ y \\ z \end{bmatrix}_{\text{MOC}} . \tag{2.5}$$

MEI to MRX mei2mrx.m makes in fact five different rotations a once. It turns the x-axis from the Earth's vernal equinox to the vernal equinox of Mars and also turns the z-axis from the Earth's spin axis to the spin axis of Mars. The entire rotation matrix can be seen in Appendix A.2.

MRX to MEO mrx2meo.m makes the coordinate system into a rotating frame by rotating around the z-axis until the x-axis turns from Mars' vernal equinox to the prime meridian ($longitude = 0$) of Mars. This is done by multiplying the MRX-coordinates with the rotation matrix R. The time-dependant angle, W, to rotate is calculated as $W = 176.634 + 350.89198226 \cdot (jd - 2451545)$, where jd is the Julian day number of when the angle should be calculated and 2451545 is the Julian day number of 1 Jan 2000 at 12.00 [Duxbury et al., 2001],

$$\begin{bmatrix} x \\ y \\ z \end{bmatrix}_{\text{MEO}} = \big[R(W)\big] \begin{bmatrix} x \\ y \\ z \end{bmatrix}_{\text{MRX}} . \tag{2.6}$$

MEO to Areographical meo2longlat.m calculates the longitude (ϕ) and latitude (λ) from the position coordinates in the MSO frame. The latitude goes from 90° at the north pole down to −90° at the south pole. The longitude is positive in east direction and starts from 0° at the Airy-0 crater,

$$\lambda = \arctan \frac{z_{\text{MEO}}}{\sqrt{x_{\text{MEO}}^2 + y_{\text{MEO}}^2}} \tag{2.7}$$

$$\phi = \begin{cases} \arccos \frac{x_{\text{MEO}}}{\sqrt{x_{\text{MEO}}^2 + y_{\text{MEO}}^2}} & \text{if y} > 0 \\ 360^\circ - \arccos \frac{x_{\text{MEO}}}{\sqrt{x_{\text{MEO}}^2 + y_{\text{MEO}}^2}} & \text{otherwise} \end{cases} . \tag{2.8}$$

Spherical to Cartesian Bfield_sph2xyz.m transforms vectors (e.g. the magnetic field vectors) from spherical components (r, θ, φ) into Cartesian components (x, y, z) [Råde and Westergren, 1998],

$$\begin{cases} \mathbf{e}_x = \mathbf{e}_r \sin\theta \cos\varphi + \mathbf{e}_\theta \cos\theta \cos\varphi - \mathbf{e}_\varphi \sin\varphi \\ \mathbf{e}_y = \mathbf{e}_r \sin\theta \sin\varphi + \mathbf{e}_\theta \cos\theta \sin\varphi + \mathbf{e}_\varphi \cos\varphi \\ \mathbf{e}_z = \mathbf{e}_r \cos\theta - \mathbf{e}_\theta \sin\theta \end{cases} . \tag{2.9}$$

As mentioned above, there are different bodies whose positions need to be described in - and transformed between - these different coordinate systems. The Rosetta spacecraft itself, the planet Mars, its two Moons (Phobos and Deimos) and the Sun must all be correctly positioned in space. It is also necessary to determine the magnetic field vectors of Mars (see Chapter 4) and the spin axis of Mars in certain systems. However, all raw trajectory/position/vector components data come from different sources and will need to follow different transformation paths. The following list describe the different transformation paths.

Rosetta Rosettas trajectory coordinates are received in MEI and follow the transformation path:

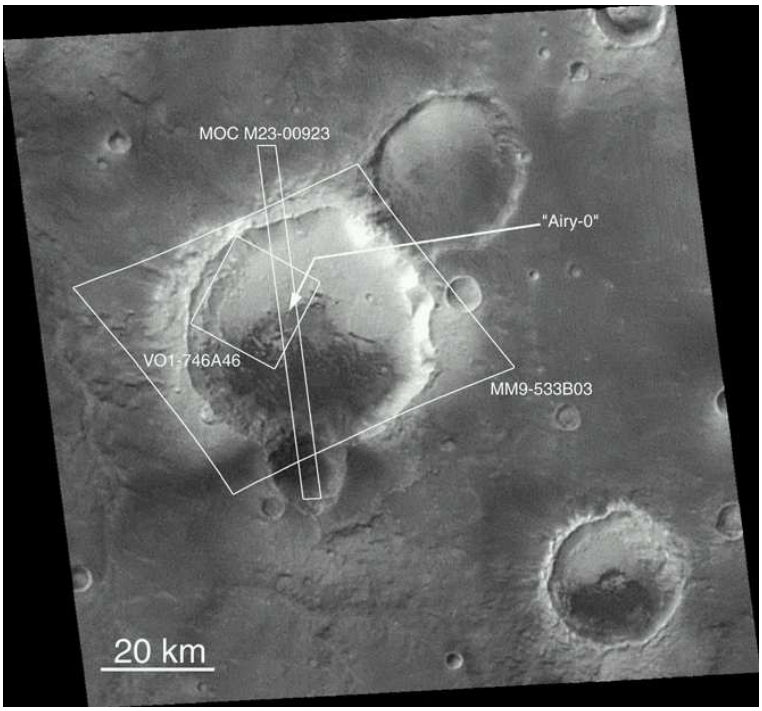

Figure 2.1: The Airy-0 crater on Mars which defines the position of the prime meridian (Longitude = 0°). Picture from NASA Jet Propulsion Laboratory.

MEI to MEA to MEC to MOC to MSO and

MEI to MRX to MEO to Areographical.

The Sun, Mars, Phobos and Deimos The positions of these four bodies are received in GEA and follow the path:

GEA to MEA to MEC to MOC to MSO.

The magnetic field vectors These vectors are calculated as spherical components in MEO and are first transformed into cartesian components. They then follow the path:

MEO to MRX to MEI to MEA to MEC to MOC to MSO

2.2 The Trajectory

The Rosetta trajectory is plotted in the MSO system in both 3D and 2D in Figure 2.2 and Figure 2.3. The spacecraft will approach Mars from the dayside and make a swing-by on the negative y-side of Mars and proceed through the tail. On its way it will cross all important plasma boundaries and layers. The bow shock will be passed at about 01.45 UT and approximately two hours later (highly dependant on the current space

weather) the S/C will cross the bow shock again, outbound. The closest approach will take place at 01.55 UT and the minimum altitude reached will be about 250 km. The total time within the ionosphere of Mars will be on the order of minutes.

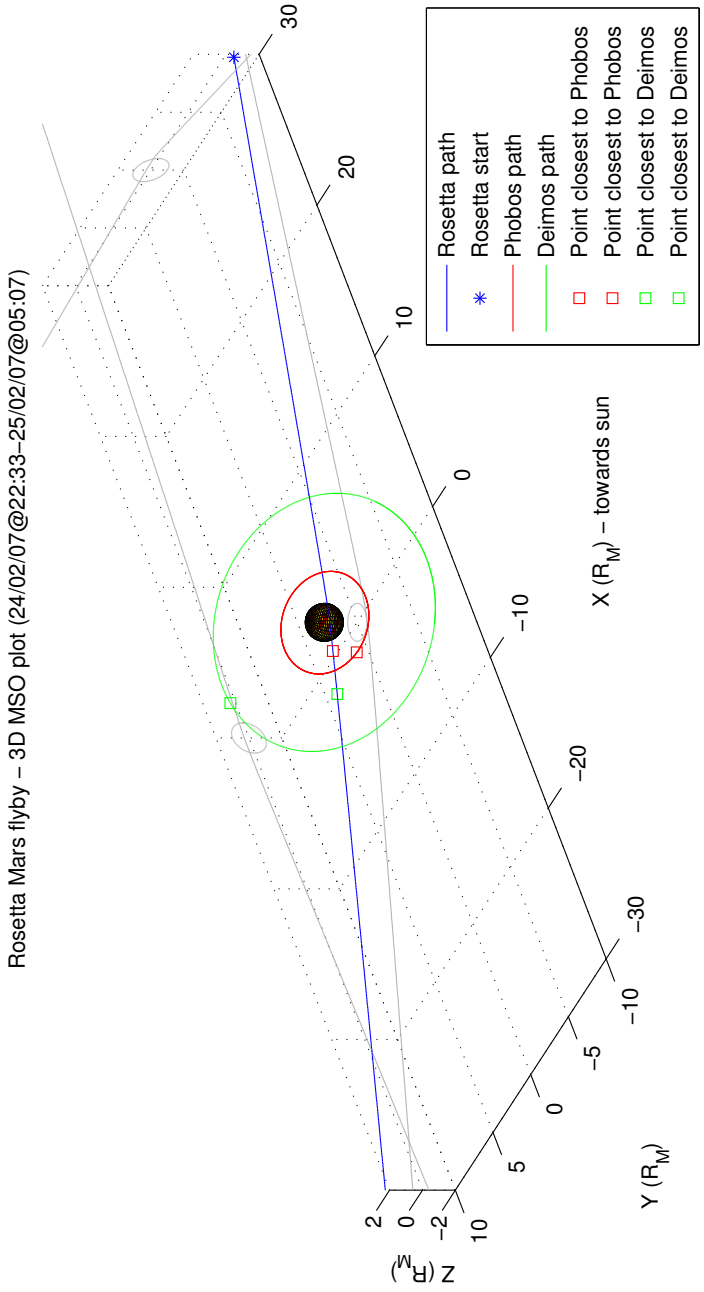

Figure 2.2: 3D view of the Rosetta trajectory (blue line) in the MSO system with the projections on the X/Y, X/Z and Y/Z plane (grey lines). Rosetta will approach Mars on the dayside (blue star indicates start of Rosetta) and proceed out through the tail. The paths of Phobos and Deimos (red and green curve, respectively) are also plotted.

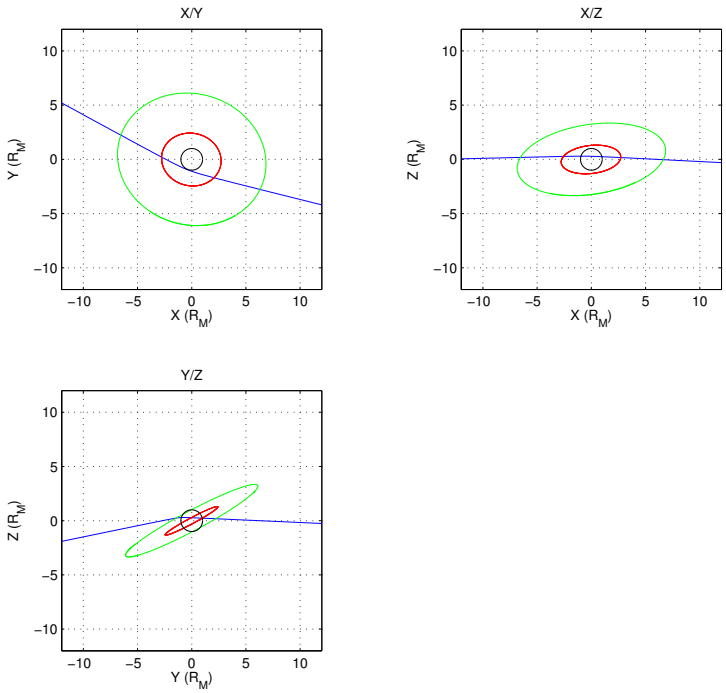

Figure 2.3: 2D views of the Rosetta trajectory (blue line) in the MSO system. The paths of the two moons, Phobos and Deimos, are plotted in green and red, respectively.

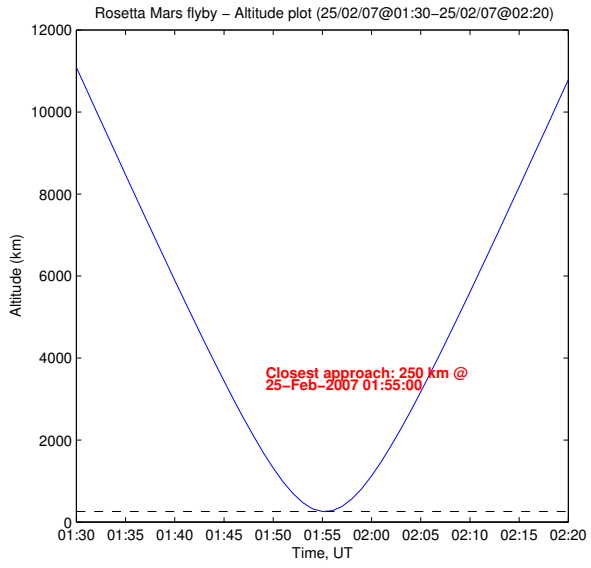

Figure 2.4: The altitude of Rosetta as function of time during the Mars flyby. The lowest altitude is indicated by the dashed line.

2.3 Mars-Sun Eclipse

When Rosetta approaches Mars, from the dayside, it has been in constant sunlight since the launch in 2004. When passing Mars, swinging by with the closest approach on the nightside, it will enter a region of shadow. In Figure 2.5 the trajectory is plotted in MSO coordinates and the time in shadow is indicated by black stars. To find out how long this eclipse will last, a simple algorithm was used. The conditions on the coordinates for a Mars eclipse are as follows:

$$x_{Rosetta} < 0 \tag{2.10}$$

and

$$\sqrt{y^2_{\text{Rosetta}} + z^2_{\text{Rosetta}}} < R_{\text{Mars}} \tag{2.11}$$

where x_{Rosetta} is the x-coordinate of Rosetta in the MSO reference frame and x_{Mars} is the x-coordinate for Mars. R_{Mars} is the radius of Mars.

By checking all position coordinates of Rosetta for these conditions, the time in shadow behind Mars was found to be 24 minutes, see Figure 2.5.

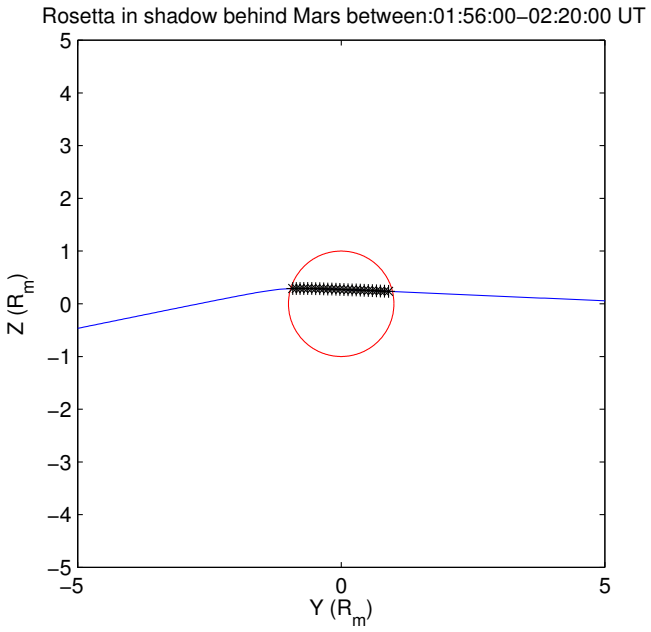

Figure 2.5: Rosetta will be in shadow behind Mars for about 24 minutes during the flyby. The reference system is MSO, the x-axis pointing out of the paper. The black stars indicate the time in shadow, the blue line is Rosettas trajectory and the red circle is Mars.

2.4 Multi-Spacecraft Opportunities

At the time when Rosetta passes by Mars, there will be no less than four additional spacecraft in orbit around Mars. Mars Global Surveyor has been there since 1997 and will be in its tenth year during the Rosetta Mars Flyby. Mars Odyssey and Mars Express was launched in 2001 and 2003, respectively. Mars Reconnaissance Orbiter has not yet arrived at Mars, but was launched on 19th October 2005 and will arrive in March 2006, about a year prior to Rosettas arrival.

This quite extraordinary clustering of spacecraft at Mars give rise to interesting possibilities for multi-spacecraft measurements. Rosetta has its entire plasma consortium, the most complete plasma package ever at Mars. Mars Global Surveyor has its magnetometers and Mars Express carries the ASPERA-3 instrument for ion measurements. Mars Odyssey and Mars Reconnaissance Orbiter do not carry any plasma instruments. If it would be possible to synchronise the plasma measurements on Rosetta, Mars Express and Mars Global Surveyor it would be an unique opportunity for multi-spacecraft plasma measurements.

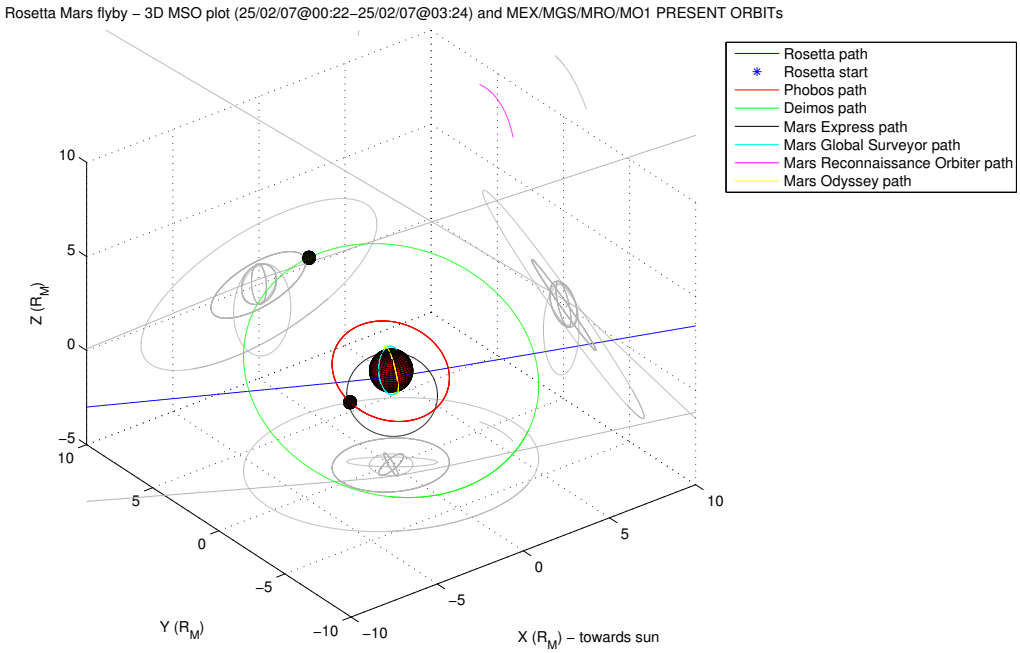

Figure 2.6: Possible trajectories of five different spacecraft during the Rosetta flyby. Two ESA missions and three NASA missions: Rosetta, Mars Express, Mars Global Surveyor, Mars Reconnaissance Orbiter and Mars Odyssey. The projections in the different planes (X/Y, X/Z and Y/Z) are included (grey lines). Additionally, the two Rovers Spirit and Opportunity are driving around on the surface (Not plotted!).

In Figure 2.6 the current trajectories of the five spacecraft are plotted. However, these

trajectories are preliminary since there could be corrections and changes to the spacecraft's orbits. This is just one example of how it could look next year based on the trajectories of today. In Figure 2.7 the projections of these trajectories are plotted.

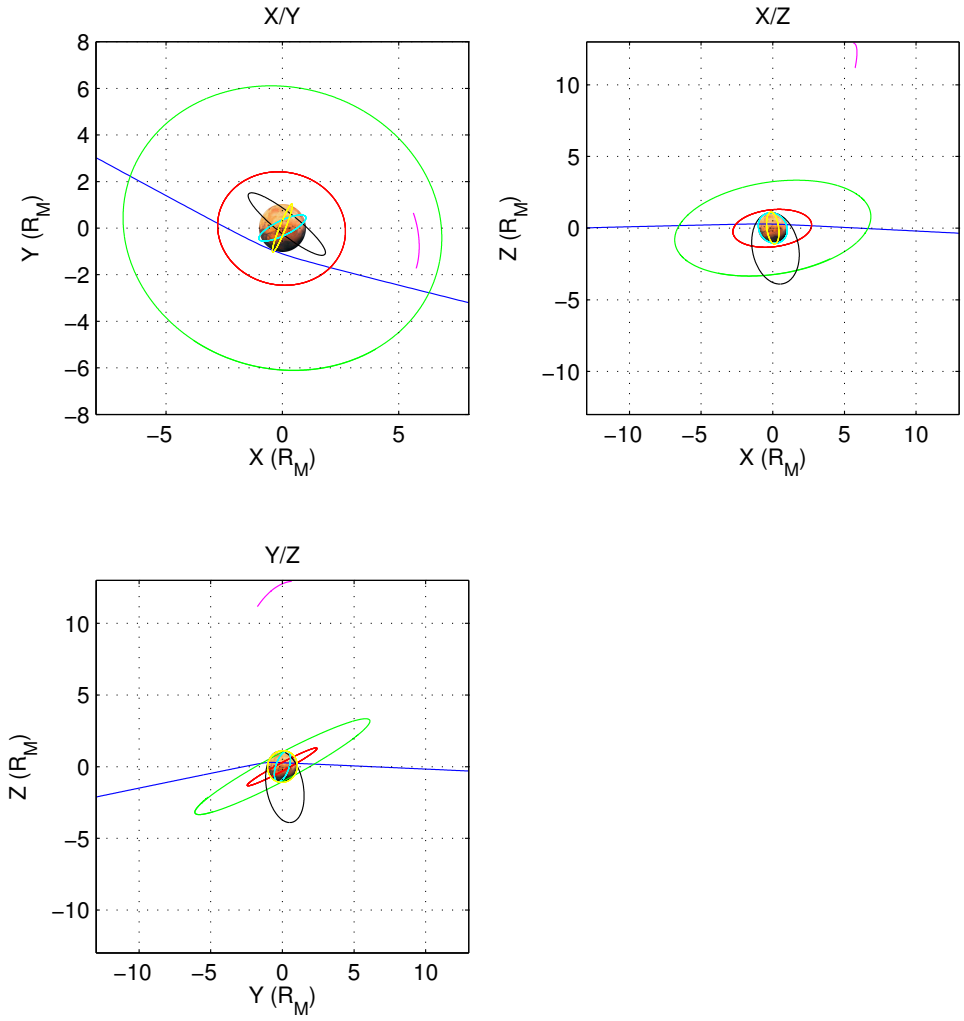

Figure 2.7: 2D projections of the current trajectories of Rosetta, Mars Express, Mars Global Surveyor, Mars Reconnaissance Orbiter and Mars Odyssey as well as of Phobos and Deimos.

Chapter 3

The Martian Plasma Environment

In the following chapter the Martian plasma environment will be explained and described. In the past, the structure of this environment with its boundaries and regions was not well known, and consequently several different names have been introduced for features that later have been understood to be identical. We will define the different boundaries and regions and use the standardised names which mainly follows the notations from Nagy et al., [2004]. We will also use the results of an existing multi-species hybrid simulation and cross-run the simulation data with Rosetta's trajectory in order to find out what Rosetta will encounter.

3.1 General Characteristics of the Plasma Environment

The structures and features of the entire plasma environment around a planet are formed when the solar wind is obstructed by the ionosphere/magnetic field or the body itself. The exact nature of the solar wind interaction with Mars have been elucidated with the recent observations of magnetic fields at low altitudes, observations by the spacecraft Mars Global Surveyor (MGS). The planet does not possess an intrinsic magnetic field but rather crustal magnetic sources which do not affect the global interaction between the solar wind and Mars [Acuña et al., 1998]. Thus the solar wind interacts directly with the upper atmosphere and the ionosphere of the planet, which is in many ways similar to a Venus-like interaction. Mars Global Surveyor has provided an illustrative map of the plasma environment, see Figure 3.1. The Phobos-2 spacecraft also gave a global picture of the plasma environment, see Figure 3.2.

At Mars, the first boundary that builds up by the super-sonic solar wind is as usually called the **bow shock** (BS). The solar wind plasma is at this boundary slowed down to sub-sonic levels and is heated. The region between the bow shock and the **magnetic pile-up boundary** (MPB) has been called the **magnetosheath** [Trotignon et al., 2000].

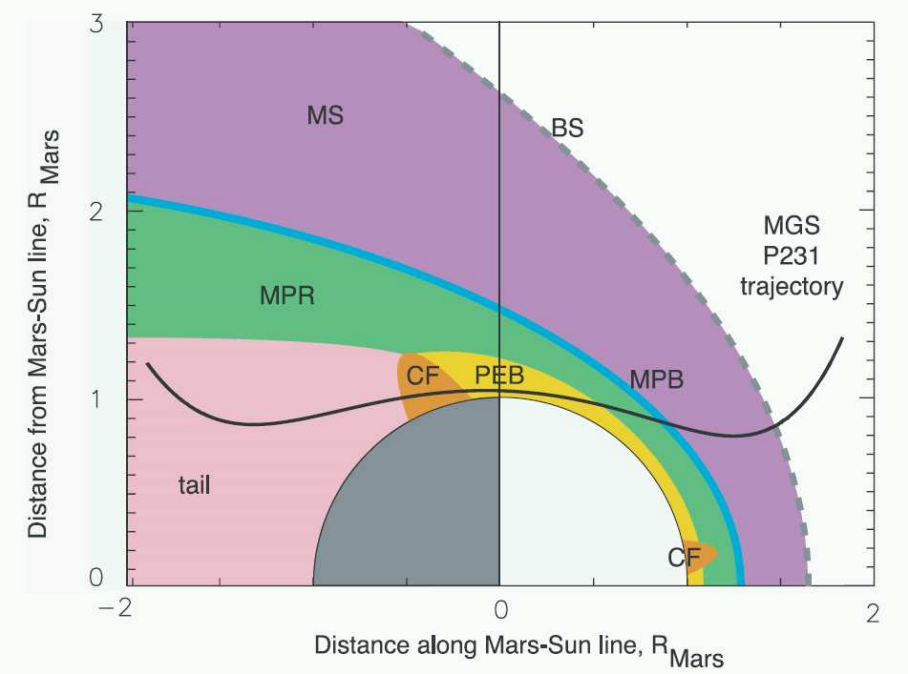

Figure 3.1: The Mars Global Surveyor has helped provide this figure of the plasma environment of Mars. The dashed line represents the bow shock, the coloured areas represents the magnetosheath (purple), magnetic pileup boundary (blue), magnetic pileup region (green), photoelectron boundary (yellow), crustal field ,CF, (orange) and tail (pink). Figure from Crider et al., [2003].

The magnetic pile-up boundary separates the heated solar wind plasma from the **magnetic pile-up region**. However, MPB, which refers to an increase of magnetic flux from the solar wind is not the only name for this region, since it has many features. It has also been called the "magnetopause" (MP), which refers to an obstacle with a weak magnetic field, "planetopause", which refers to a boundary separating the solar wind/sheath plasma from the inner **magnetic tail** and the "magnetic flux pile-up boundary" or just "magnetic pile-up boundary" (MPB). The acronym MP can therefore either mean "magnetopause" or "magnetic flux pile-up" but refers to the same boundary [Lundin and Barabash, 2004]. Trotignon et al., [2000], give a few more names for the MPB: the "protonopause" or the "ion-composition boundary", describing it as the region which separates the shocked solar wind protons from O^+-ions of Martian ionospheric origin. It is also seen as the disappearance of the high levels of electric and magnetic turbulence characterising the magnetosheath as well as an increase in the plasma density. The name suggested as standard by for this feature is the magnetic pile-up boundary [Nagy et al., 2004].

The features in the magnetic pile-up region region can be summarized as follows: the magnetic field piles up and there is a drop in the magnetic field fluctuations compared to the magnetosheath [Nagy et al., 2004]. Their is as well a strong enhancement of the magnetic field around the planet [Bertucci et al., 2003]. The solar wind proton density

decreases while the planetary ions increase. There is also a sharp increase in electron density while the electron temperature drops. Localised high-frequency emissions appear. The MPB and MPR are permanent features of the interaction and the two interaction mechanisms that could account for all or part of these characteristics are charge exchange and mass loading [Nagy et al., 2004].

Øieroset et al., [2004], talks about a possible **plasma depletion layer** (PDL) in some parts of the magnetic pile-up boundary. A PDL means a region where the density goes down and an increase in electron fluxes occur.

Crider et al., [2003], talks about a **photoelectron boundary** (PEB) just inside the MPR. In this region electron fluxes are dominated by locally produced photoelectrons in the range 10 eV to 20 keV. Above the PEB, cooled electrons from the solar wind dominate.

Somewhere in the magnetosheath, between the bow shock and the magnetic pile-up boundary lies the **mass-loading boundary** (MLB). Inside this layer, the ionisation of neutral particles is increased and as these ions are being accelerated, due to the $\mathbf{v} \times \mathbf{B}$-drift, a mass-loading region is created [Lundin and Barabash, 2004]. The entire region within the MPR is called the **magnetosphere** [Nagy et al., 2004].

The innermost feature of the plasma environment is the **ionosphere** which for the Earth and Venus for instance ends with an **ionopause**, characterised by a sudden drop in plasma density [Nagy et al., 2004]. This has not been distinctly found at Mars but according to Acuña et al., [1998], there is an ionopause at an altitude of 300-500 km from the planet surface, characterised by a sudden drop in the electron flux.

Grard et al., [1991], uses the terms "planetopause", "planetosheath" and "planetosphere" instead of "magnetopause" etc. but the prefix "planeto" will not be used in this report.

3.2 A Martian Plasma Environment Dictionary

A small Martian Plasma Environment dictionary is presented below to summarise the features of the main regions and boundaries and their names.

Bow shock (BS) Slows down the super-sonically flowing solar wind.

Ion-composition boundary See Magnetic pile-up boundary.

Ionosphere The uppermost ionized region of the atmosphere. Fractions of matter in ionized state increases with altitude to a density peak and then decreases.

Ionopause The boundary that ends the ionosphere, with a sudden drop in electron flux. A sudden drop in plasma density is not yet really observed.

Magnetic pile-up region (MPR) The region where the interplanetary magnetic field gets stronger (piles up) before it slowly gets weaker (diffuses), among many other features.

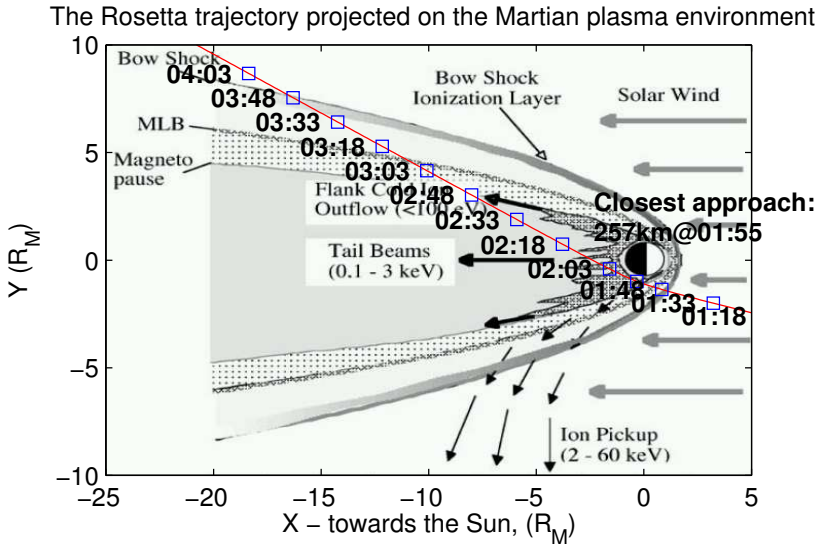

Figure 3.2: The Phobos-2 spacecraft provided a global picture of the Martian magnetosphere [Lundin and Barabash, 2004]. The Rosetta trajectory is included (red line) and every 15th minute is indicated with a blue square. The closest approach of about 250 km will take place at 01.55.

Magnetic pile-up boundary (MPB) Separates the shocked solar wind plasma (magnetosheath) from the magnetic pile-up region. Also known as the magnetopause, planetopause, protonopause or ion-composition boundary (ICB).

Magnetopause See Magnetic pile-up boundary.

Magnetosphere The entire region within the MPR. Also known as the planetosphere.

Magnetosheath The region between the bow shock and the MPR. Also known as the planetosheath.

Magnetotail/Central tail The plasma region behind the planet as seen from the Sun.

Mass-loading boundary (MLB) Situated between the bow shock and the MPR. Below the MLB ionospheric ions are being accelerated and mass-loading take place.

Photoelectron boundary (PEB) A boundary suggested to exist just below the magnetic pile-up boundary, characterised by a domination of photoelectrons.

Plasma depletion layer (PDL) A region upstream of the magnetic pile-up boundary where an increase in electron flows take place.

Planetopause See Magnetic pile-up boundary.

Planetosheath See Magnetosheath.

Planetosphere See Magnetosphere.

Protonopause See Magnetic pile-up boundary.

3.3 Ionospheric Models

In the following section we summarize some previous ionospheric models. Previous measurements of the plasma environment of Mars are not very numerous since only a few of the spacecraft that have ever visited Mars have had adequate instruments onboard (see Section 1.3). The five most valuable missions for plasma measurements were the two Viking landers, Mars Global Surveyour, Phobos-2 and Mars Express. In-situ measurements from the two Viking landers are shown in Figure 3.3 and Figure 3.4.

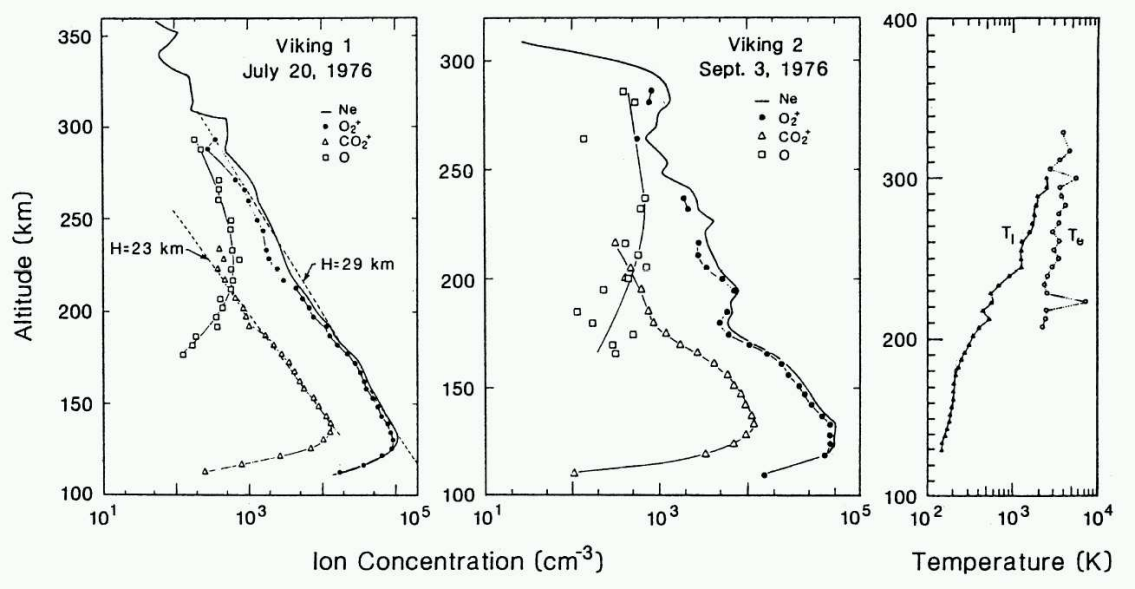

Figure 3.3: Ion density and electron (T_e) and ion (T_i) temperature profiles from the two Viking landers. Figure from Trotignon et al., [2000].

Ionosphere models can of course be more or less accurate depending on what theory that lies behind. A good safety procedure would be to study many different models and therefore get a more reliable range of possible values (such as density profiles and temperature profiles). There are roughly two different types of models, three-dimensional global circulation models (GCMs) which include horizontal transport of gas and plasma, and one-dimensional models which only include vertical variation and transport, but can include more accurate description of physical and photochemical processes.

In the following subsections, we will describe four different models of the ionosphere and show some of their results.

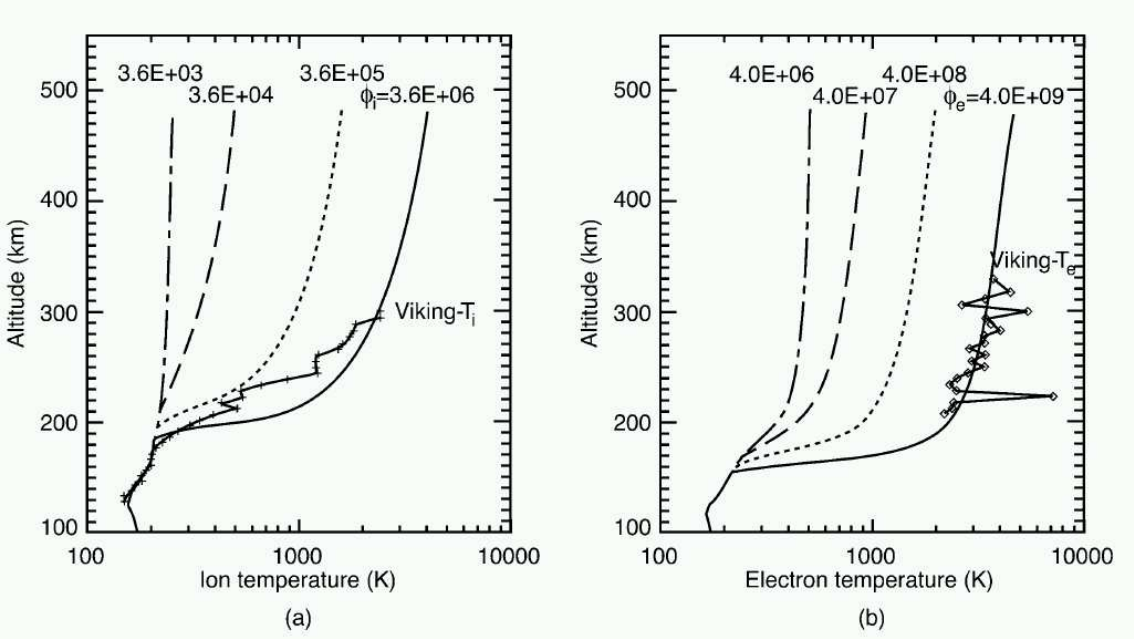

Figure 3.4: Electron and ion temperatures from Viking 1 together with modelled profiles. Figure from Nagy et al., [2004].

3.3.1 The MarTIM Model

The first model we study is the Martian thermosphere and ionosphere global circulation model (MarTIM) [Moffat, 2005]. MarTIM covers an altitude range of 60 – 250 km and self-consistently calculates the composition of the three main gases, CO_2, N_2, and O. The minor gases CO, Ar, O_2 and NO, are based on diffusive equilibrium above the turbopause. The ionosphere is calculated from a simple photoionisation and charge exchange routine. The lower boundary in this model was altered using output from the Mars Climate Database.

Ion density profiles and electron density profiles are shown in Figures 3.5 and 3.6.

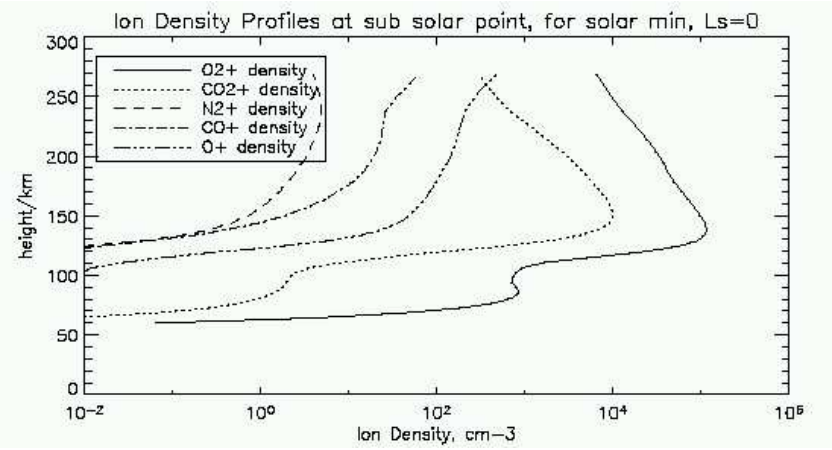

Figure 3.5: Ion density profiles for five different ions in the Martian ionosphere from the MarTIM model, with solar minimum and equinox conditions at the sub-solar point. Figure from Moffat, [2005].

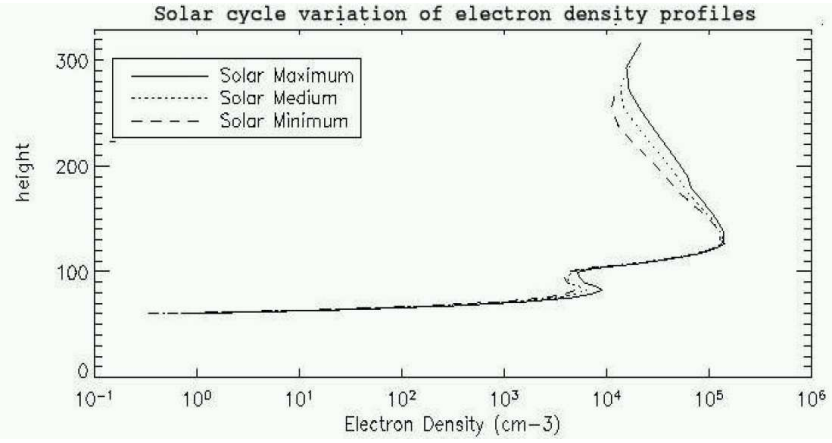

Figure 3.6: Electron density profiles in the Martian ionosphere from the MarTIM model, with varying solar intensity. Figure from Moffat, [2005].

3.3.2 The MTGCM model

Another GCM is the Mars thermospheric general circulation model (MTGCM). It is based on a model for Earth's thermosphere but was adapted for Mars in 1988. It is a finite difference, time-dependent, primitive equation model that self consistently and numerically solves for thermospheric neutral temperatures, neutral and ion densities and a three-dimensional wind field and covers an altitude range of 70–300 km.

This model has been used by Fox et al., [1996], to study the variations of the thermosphere/ionosphere at high and low solar activities. Density profiles for several different ions as well as electrons were produced and can be seen in Figures 3.7 and 3.8.

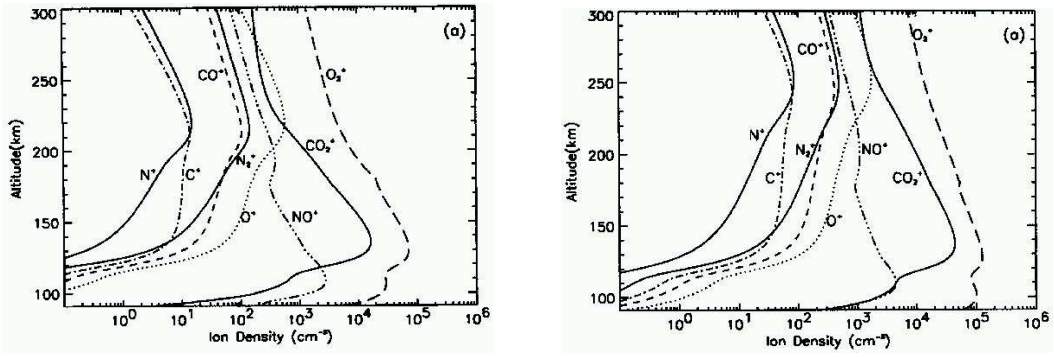

(a) Low solar activity

(b) High solar activity

Figure 3.7: Density profile for ions in the Martian ionosphere at low (left) and high (right) solar activity, computed with MTGCM. Figure from Fox et al., [1996].

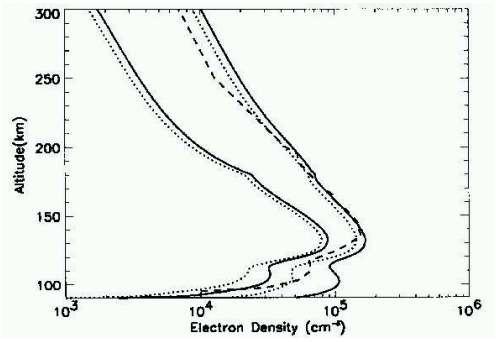

Figure 3.8: Solid curves: Density profile for electrons in the Martian ionosphere at high (right) and low (left) solar activity with solar fluxes from W.K. Tobiska, computed with MTGCM. The dotted curves were calculated using solar fluxes from H.E. Hinteregger. The dashed curve is the electron density profile derived from the Mariner 6 radio occultation measurements. Figure from Fox et al., [1996].

An interesting conclusion from Fox et al., [1996], is that the ionosphere is predicted to show a substantial variation in both peak densities and scale heights due to the solar

activity [Fox et al., 1996].

3.3.3 3D three-species MHD model

The Martian interaction with the solar wind has also been modelled by Liu et al., [2001], in order to observe the general features of the bow shock and ionopause. The results were found to be in agreement with averaged observations. This model uses three continuity equations to consider protons (from the solar wind) and the two dominant heavy species in the ionosphere, O^+ and O_2^+, separately. However, only one momentum equation and one energy equation is used which means that all ions have the same temperature and the same velocity.

This model is not really a model of the ionosphere but rather a global plasma environment model. However, the ionosphere is represented but not with such accuracy as the previous models. This model also provides density profiles to higher altitudes than the previous ones (as far as 1000 km) which motivates the study of it, since it is quite good to have an idea of the parameter values above the ionosphere. Liu et al., [2001], also studied the effects of a surface crustal magnetic field on the bow shock and ionosphere. The Mars Global Surveyor measurements have shown that Mars has no significant global intrinsic magnetic field but several small, local crustal magnetic field anomalies (see Chapter 4). Adding this crustal magnetic field to the model turns out to have a great impact on the electron density profile as can be seen in Figure 3.9.

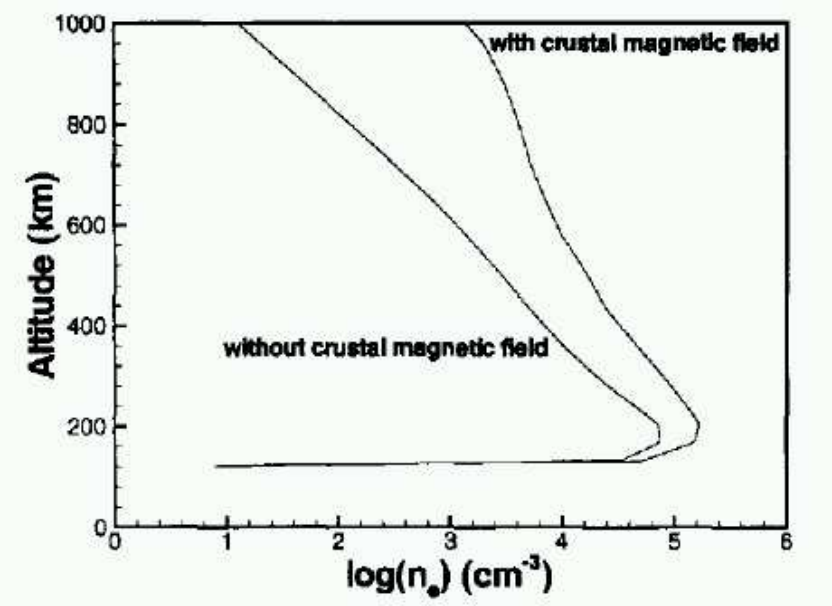

Figure 3.9: Electron density profile in the Martian atmosphere with and without a crustal magnetic field. The crustal field, a dipole with magnetic moment of $2.6 \cdot 10^{17}$ Am^2, was positioned at 45°S (latitude of 45 degree in the southern hemisphere). Figure from Liu et al., [2001].

3.3.4 Simple Photochemical Model

Martinis et al., [2003], have used a simple photochemical model of Mars' ionosphere to investigate day-to-day changes in the electron density profile up to an altitude of 200 km. They assumed that the only varying parameter is the solar irradiance and compared their calculations to Mars Global Surveyor data for the period 9–27 March 1999. By comparing Figure 3.10 (a) and (b) it can be seen that the model is in agreement with measurements.

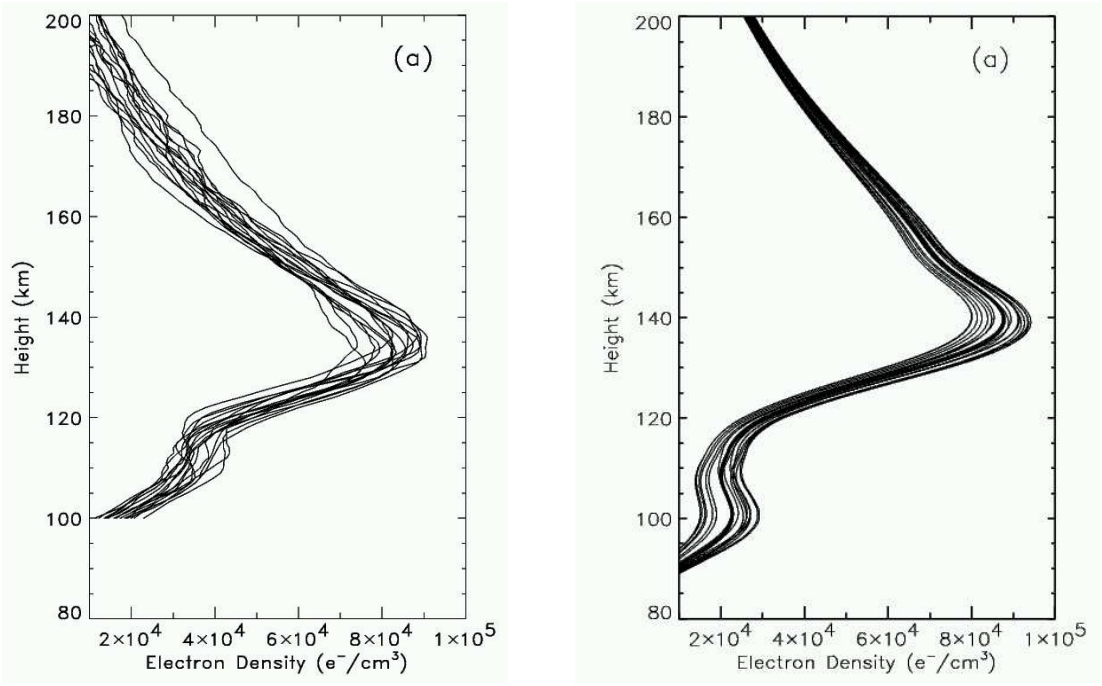

(a) MGS measurements

(b) Model results

Figure 3.10: Electron density profiles from 9–27 March 1999 as observed by the MGS satellite (left) and as calculated from the model (right). Figure from Martinis et al., [2003].

The variations in electron density can be up to 19% in the model and up to 10% according to MGS data [Martinis et al., 2003].

3.3.5 Ionospheric Plasma Expected for Rosetta

Summarizing the results from the ionosphere models we find that Rosetta, with a closest approach of 250 km, will experience a maximum electron density of approximately $2 \cdot 10^4$ cm^{-3}. The combined ion density should reach the same values. The electron temperature, decreasing towards to the planet, should reach an approximate value of 2000 K (or

0.17 eV) while the ion temperature should reach about 3000 K (or 0.26 eV).

3.4 Using a 3D Simulation

In order to actually get some quantitative predictions on what Rosetta might encounter during its flyby a 3D multi-species hybrid simulation of the Martian plasma environment from Modolo et al., [2005], has been used. There are several other simulation models for the Martian plasma environment but as Ronan Modolo, postdoc at IRFU, kindly agreed to provide the results from the model developed by him and G.M Chanteur for this study, this is the model used here. Most of the studies using this model have been done in collaboration with Ronan Modolo. By using this 3D simulation it is possible to get the values of certain parameters (such as densities and magnetic field) at any specific point in the vicinity of Mars. This specific point can for instance be a Rosetta trajectory coordinate. By "cross-running" all the Rosetta coordinates, which are defined for every minute, with the simulation data we get time series of plasma parameters. All calculations with this model have been done using IDL.

3.4.1 Model Description

This multi-species hybrid model uses a fixed cartesian-grid with a spatial resolution of 300 km in which the dynamics of several ion species and the interplanetary magnetic field are represented. The electrons are taken into account as a passive fluid to ensure the conservation of quasi-neutrality in the plasma. It is therefore not possible to draw any conclusion on the electron temperature from the model data.

A neutral exosphere model is also included, which means that there is an oxygen (thermal-/suprathermal) and hydrogen neutral corona, acting as a source for the planetary plasma. The ionisation processes included are photo ionisation, ionisation by electronic impacts and charge exchange reactions.

The crustal magnetic field of Mars is not included, only the interplanetry magnetic field (IMF). The interplanetary magnetic field has no sunward component, meaning that the magnetic field lines are perpendicular to the direction of the Sun. However, the clock angle of the interplanetary magnetic field is arbitrary since there is no other asymmetry in the model.

Solar minimum conditions are assumed for the solar UV flux and the oxygen and hydrogen corona (in 2007 there should be a minimum in the 11-year solar cycle).

The solar wind is assumed to a have a density of 2.3 cm^{-3} and to a have a speed of 400 km/s. The composition of the solar wind is 95% H^+ and 5% He^{2+} by number. The IMF has a strength of 3 nT.

The coordinates used in the simulation are similar to MSO, but with the x-axis pointing away from the Sun. The z-axis is as in MSO along Mars orbital momentum vector but the y-axis is opposite to $\hat{y}_{\mathrm{MSO}}$.

3.4.2 Simulation of the Rosetta Flyby

We plot global maps of plasma parameters such as densities, flow velocities and interplanetary magnetic field strength. On these maps, the Rosetta trajectory is projected in order to get an overview of which boundaries and regions that will be crossed, see Figure 3.11.

The values of the different plasma parameters are calculated along the Rosetta path. However, as mentioned in the model description the spacing of the simulation grid is 300 km. This means that the simulation parameter values, which are calculated for every 300 km need to be linearly interpolated in three dimensions to the exact coordinates of Rosetta.

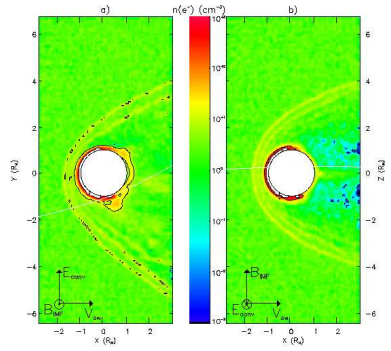

(a) X/Y and X/Z-planes.

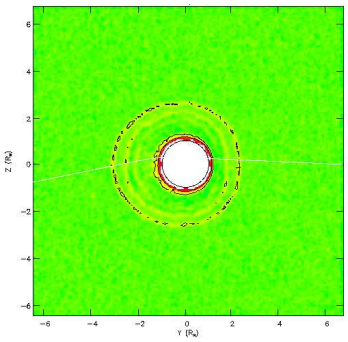

(b) Y/Z-plane.

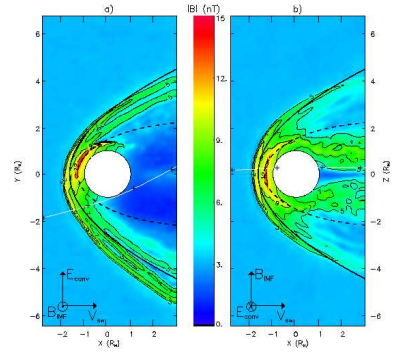

(c) X/Y and X/Z-planes.

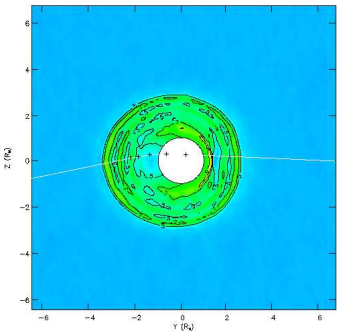

(d) Y/Z-plane.

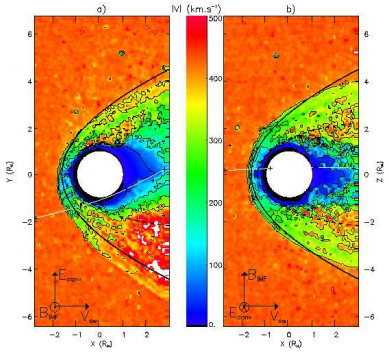

(e) X/Y and X/Z-planes.

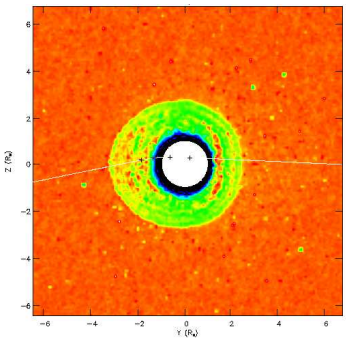

(f) Y/Z-plane.

Figure 3.11: Electron density maps (top), interplanetary magnetic field maps (middle) and plasma flow velocity maps (bottom)[Modolo et al., 2005]. Rosetta's trajectory is indicated with a white line.

When obtaining the values of different parameters from the simulations as time series, only the five major ion species are considered even though the model includes additional ions species. The species included are the two solar wind ions, hydrogen, H^+_{sw}, and helium, He^{2+}_{sw}. The planetary ions, i.e. the ions originating from Mars, are atomic oxygen ions, $O^+_{Planetary}$, molecular oxygen ions, $O^+_{2,Planetary}$ and hydrogen ions,$H^+_{Planetary}$.

It is possible to derive the electron densities as well, even though they are not present in the model as an "active" species. The plasma has to be quasi-neutral, that is, if all charges in the plasma environment are added, the total sum should be zero. Since the electrons are the only negatively charged species present, the total charge density $n(e^-)$, should be equal to the sum of all the ion charge densities,

$$n(e^-) = n(H^+_{sw}) + 2 \cdot n(He^{2+}_{sw}) + n(O^+_{Planetary}) + n(H^+_{Planetary}) + n(O^+_{2,Planetary}) \quad (3.1)$$

A strong asymmetry along the y-axis is clearly seen in Figures 3.11 (a-f), while the magnetic field, as well as the other plasma parameters, is more or less symmetric along the z-axis. Since the incoming interplanetary magnetic field can have any clock angle, depending on the space weather during the Rosetta Mars flyby, and there is no other asymmetry in the simulation, it is possible to turn the $\mathbf{B}_{IMF}$-vector around the x-axis. This is done for five different angles, which can be seen in Figures 3.12, 3.14, 3.13, 3.15 and 3.16, where there are five different lines in each plot. We have limited the rotation of the interplanetary magnetic field to 180°, showing the asymmetry with respect to the motional electric field. Note that the interplanetary magnetic field is assumed to be perpendicular to the solar wind velocity in these simulations, but it can also be tilted and then have a sun-ward component.

It is possible to calculate the kinetic energy per nucleon E_k from the simulation data by

$$E_k = \frac{1}{2} m_p \sqrt{V_x^2 + V_y^2 + V_z^2} \quad (3.2)$$

where m_p is the proton mass and V_x^2, V_y^2 and V_z^2 are the velocities of the specific ion species, with information on the bulk velocities as well as the thermal velocities. E_k therefore is the kinetic energy, including the random thermal motion. The result is shown in Figure 3.15.

The effective ion mass m_{eff} is possible to calculate as

$$m_{eff} = \frac{n_e}{\sum_{i=1}^{5} \frac{n_i}{m_i}} \quad (3.3)$$

where n_i are the densities of the ion species, m_i are the corresponding masses and n_e is the electron density. The result is shown in Figure 3.16.

3.4.3 Discussion of the Simulation Results

To summarize the results in Figures 3.12 – 3.16 we can note that the bow shock is encountered around 01:43 UT, where there is a sharp increase in the magnetic field as well as a sharp drop in the Sun-ward plasma flow velocity. Signatures of heavy ions occur before the bow shock, but their densities are small and not likely to be observed with the Langmuir probes on Rosetta. The kinetic energy drops for the solar wind ions at the bow shock, but soon increases again in the magnetosheath. For the planetary ions there are quite large oscillations all the way into the ionosphere, probably due to the lack of statistics of particles in the simulation.

The magnetosheath, where the magnetic field and plasma flow are more turbulent, is observed from about 01:43 to 01:50.

The magnetic pile-up region/boundary can possibly be seen around the sub-solar point for some clock angles as an increase in magnetic field strength at around 01:50. Due to numerical diffusion and finite grid size, the simulated magnetic field intensity is lower than the observations where the magnetic field magnitude can reach 25 – 30 nT in the magnetic pile-up region.

The ionosphere is reached at around 01:50 when there is a large drop in plasma flow velocities and an increase in planetary ion densities. The closest approach take place at 01:55, but the peak density is encountered two minutes earlier since the closest approach is on the nightside where the plasma density is lower. The main ion species is the atomic oxygen ion with an expected peak density of about $1 \cdot 10^3$ cm^{-3}. The effective ion mass increases first when entering the ionosphere.

Depending on the clock angle of the incoming interplanetary field there can be quite large variations. Some peaks in the plasma flow velocity and in the magnetic field strength occur for some angles while they are missing for others.

Rosetta leaves the ionosphere on the nightside after 9 minutes at 01:59 and enters the magnetic tail region where densities of the planetary ions decrease and the solar wind ions become dominant. The effective ion mass drops but some peaks are visible indicating that there is an outflow of heavier planetary ions.

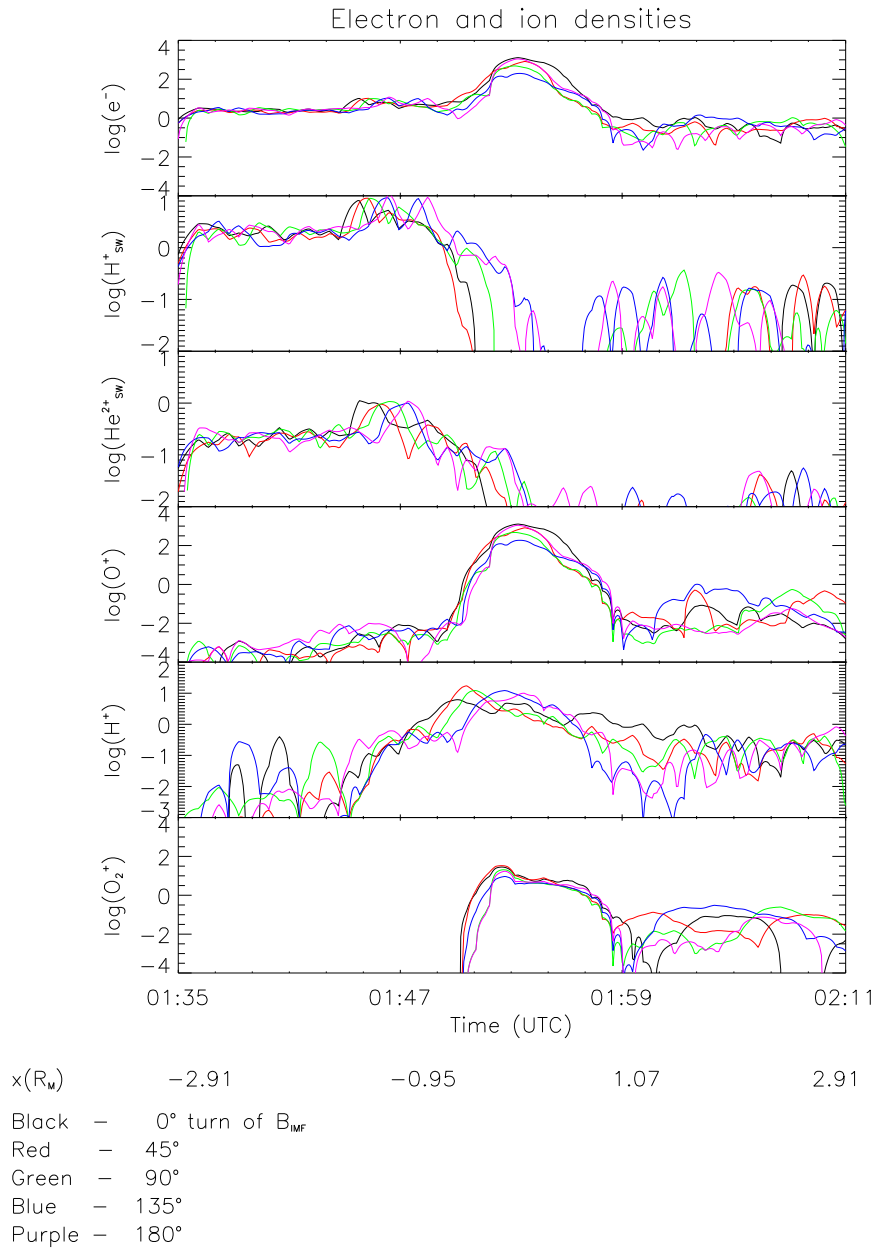

Figure 3.12: Ion and electron densities in Rosetta's path, calculated by using the 3D model of Modolo et al., [2005]. The time series are calculated for five different clock angles of the interplanetary magnetic field.

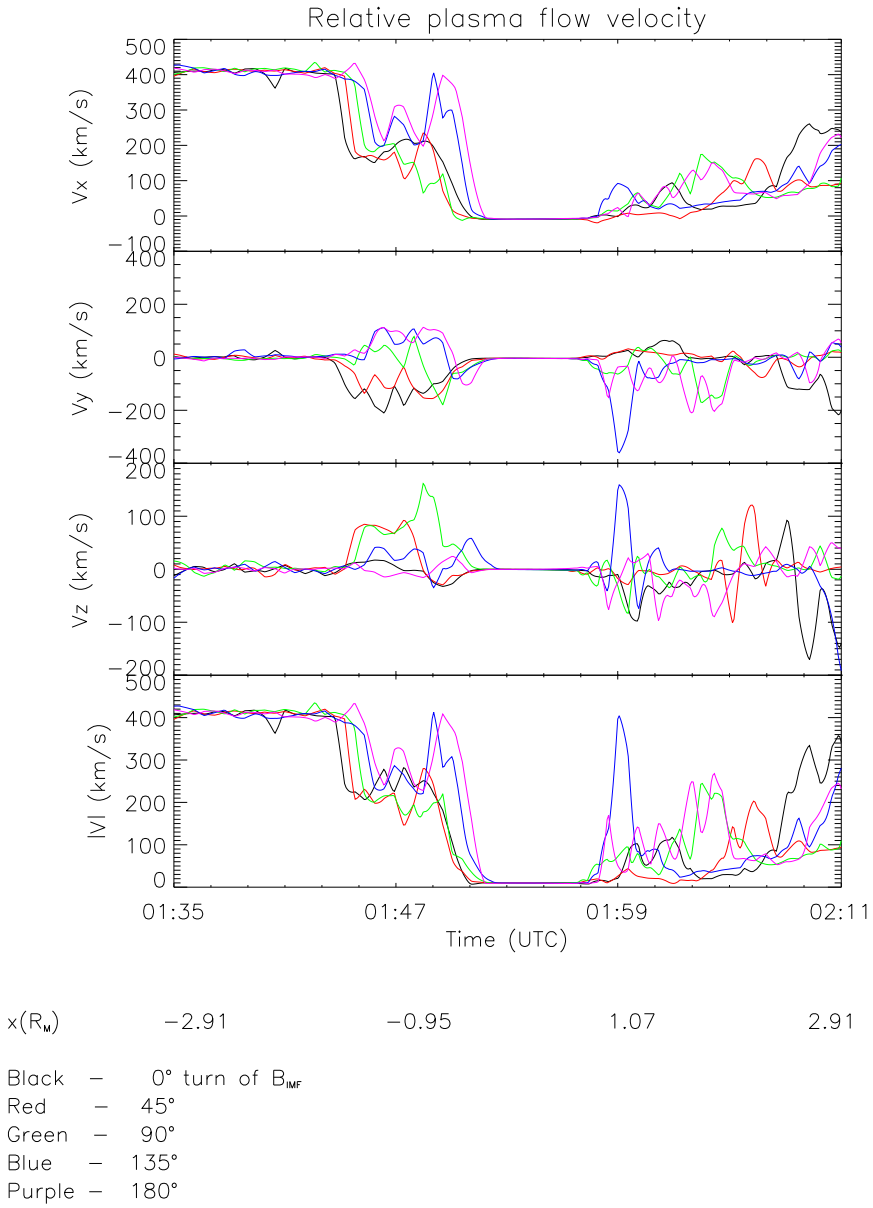

Figure 3.13: Plasma flow velocity relative to Rosetta's velocity, three components and total speed, given in the MSO coordinate system. The time series are calculated for five different clock angles of the interplanetary magnetic field.

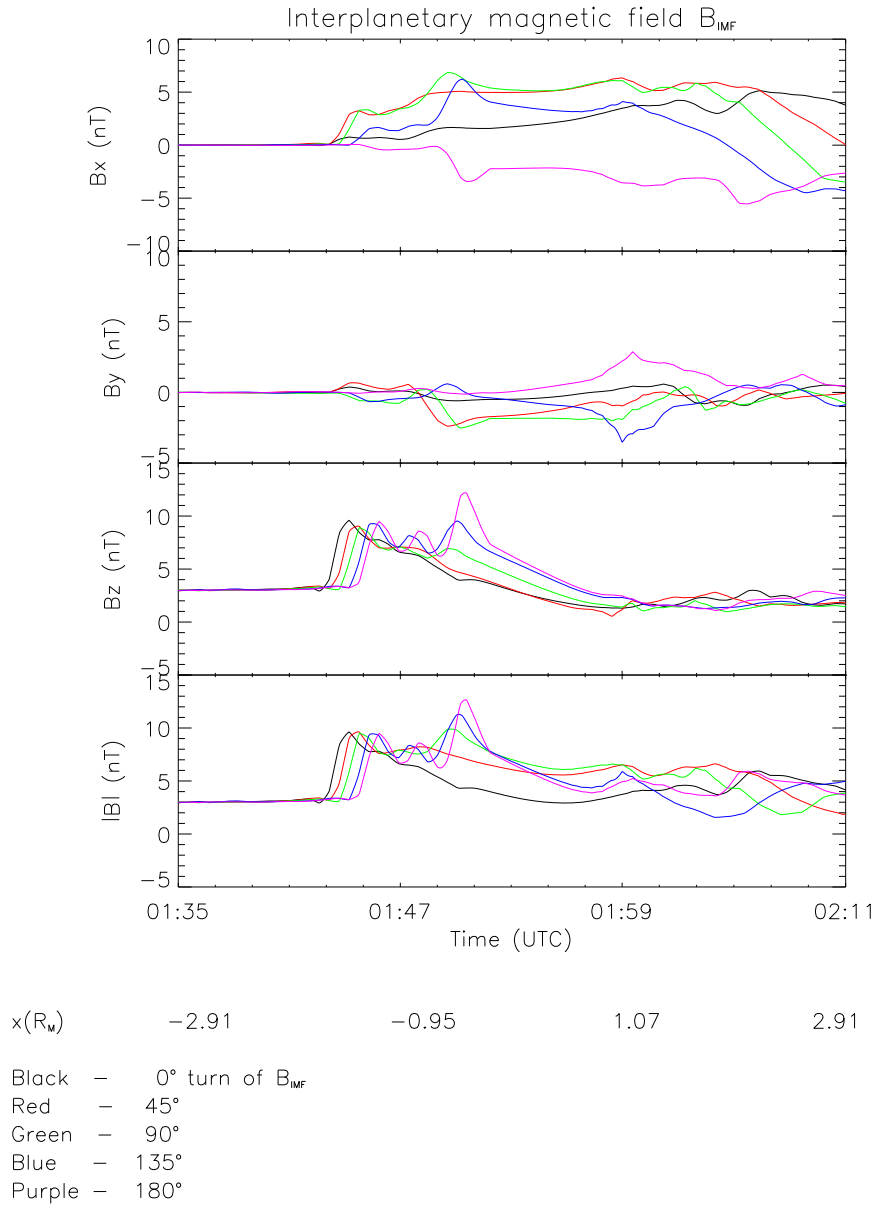

Figure 3.14: Interplanetary magnetic field in Rosetta's path, three components given in MSO and the total field strength. The time series are calculated for five different clock angles of the interplanetary magnetic field.

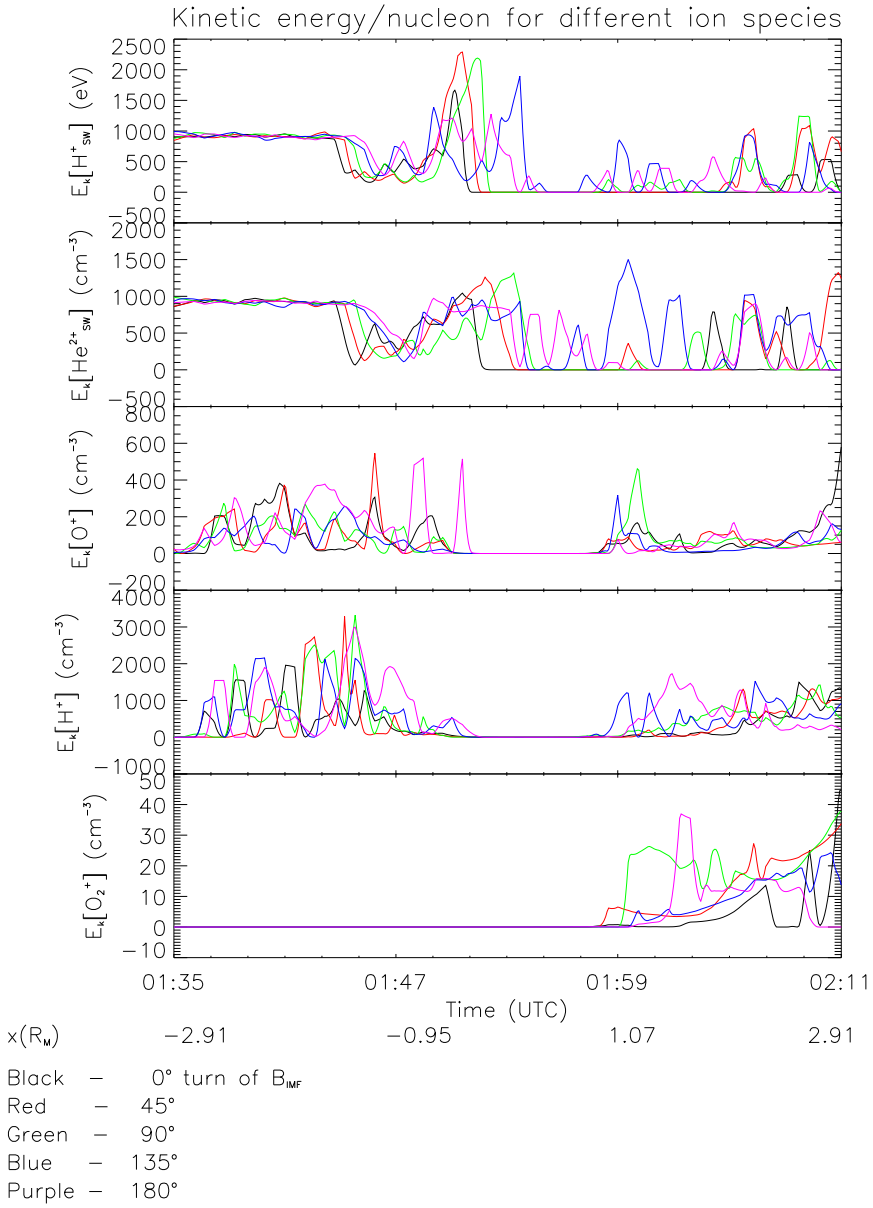

Figure 3.15: Kinetic energy per nucleon in Rosetta's path for five different ion species. The time series are calculated for five different clock angles of the interplanetary magnetic field.

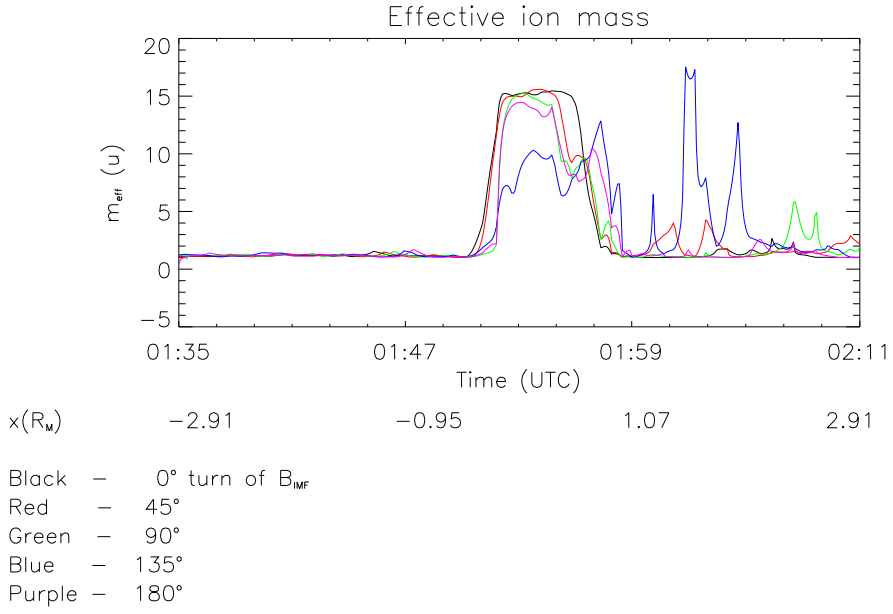

Figure 3.16: The effective ion mass for five different clock angles of the interplanetary magnetic field in Rosetta's path.

Chapter 4

The Martian Magnetic Field

The Martian crustal magnetic field will be described in this chapter. We can distinguish two sources for the magnetic field around Mars: the interplanetary magnetic field and the field of Martian origin. Mars does not possess an intrinsic magnetic field but crustal magnetic sources which have been identified recently by the Mars Global Surveyor mission [Acuña et al., 1998]. This remnant magnetic field indicates that the planet had a dynamo which is not active nowadays. The history of the dynamo of the planet, the date of its extinction, is still a major unanswered question.

This crustal magnetic field might be of great importance to Rosetta's plasma measurements since it can effect the features of the ionosphere and the entire plasma environment around the planet. It is therefore necessary to investigate. We have implemented and used one model of the crustal magnetic field, which allow us to map the crustal magnetic sources in order to find out the possible magnetic anomalies that Rosetta can fly over.

4.1 Martian Crustal Magnetic Field Models

MGS measurements showed a lot of crustal magnetic anomalies which afterwards have been nicely modelled and mapped [Arkani-Hamed, 2004], [Langlais et al., 2004], [Cain et al., 2003], [Purucker et al., 2000], and [Acuña et al., 1999]. The global magnetic field maps of Arkani-Hamed, [2004], and Langlais et al., [2004], are shown in Figures 4.1 and 4.2. All models show quite good coherence to each other, at least for the locations of the strong magnetic anomalies.

Arkani-Hamed, [2004], and Cain et al., [2003], used spherical harmonics models to produce maps, while Purucker et al., [2000], and Langlais et al., [2004], used preliminary binned magnetic field data with components in purely radial and in three directions, respectively, to produce maps.

The magnetic field strength was before the arrival of MGS believed to be weak, but recent data show that the strength on the surface is on the same order of magnitude as the magnetic field of the Earth [Langlais et al., 2004]. Figure 4.1 and 4.2 shows the

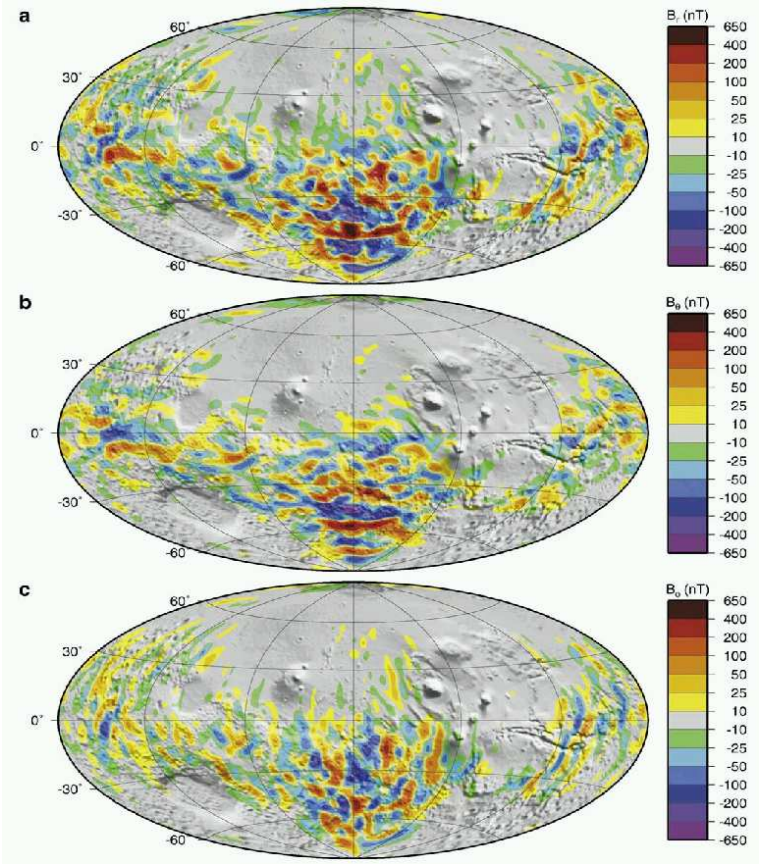

Figure 4.1: Langlais' crustal magnetic field map of Mars. The magnetic field is here calculated at an altitude of 200 km, in three components, a: r-component, b: θ-component, c: ϕ-component. Figure from Langlais et al., [2004].

magnetic field at an altitude of 370 km and 200 km, respectively. The map at 200 km has an extreme value of ± 600 nT. At the surface, the magnetic field is expected to be as strong as ± 50 μT (the magnetic field at the magnetic equator on Earth is about 30 μT [Nordling and Österman, 1999]).

However, the field of Mars does not at all resemble the Earth's dipole-like magnetic field which is generated by currents in the inner core. The magnetic field of Mars is instead very local and quite unevenly spaced. It is not generated by internal currents but rather built up by "crustal magnets" believed to be remnants of an earlier epoch when a global magnetic field existed. As can be seen in the maps, the magnetic anomalies are mainly situated in the southern hemisphere of Mars, where the surface is oldest.

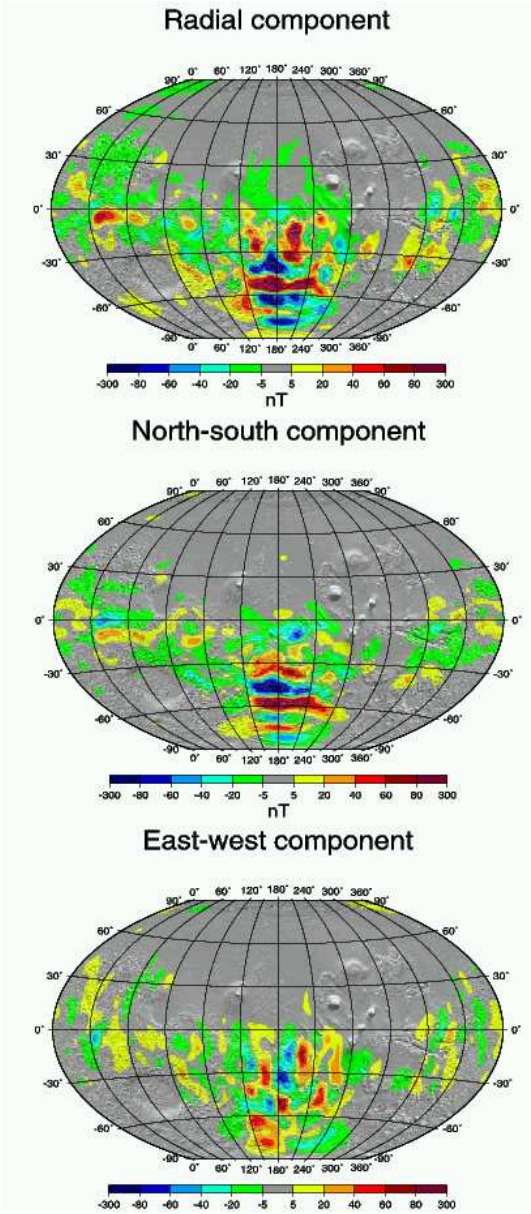

Figure 4.2: Arkani-Hamed's crustal magnetic field map of Mars. The three components of the magnetic field is calculated at an altitude of 370 km by using a 62-degree spherical harmonics model. Figure from Arkani-Hamed, [2004].

4.2 A Spherical Harmonics Model

In order to more accurately determine the crustal magnetic field which Rosetta will encounter in its path, it was decided that we should use one of the models described above to get numerical estimates of the magnetic field along Rosetta's trajectory. Jafar Arkani-Hamed was contacted and he agreed to share his model with us. As mentioned above, his model is based on spherical harmonics with coefficients determined from binned MGS data. We will first derive the expression for the magnetic field components from a magnetic potential.

The magnetic potential V at a given point (r, θ, φ) can be expressed as

$$V(r,\theta,\varphi) = a\sum_{n=1}^{N}\left(\frac{a}{r}\right)^{n+1}\sum_{m=0}^{n}[(g_{nm}\cos m\varphi + h_{nm}\sin m\varphi)P_n^m(\cos\theta)] \tag{4.1}$$

where r is the distance from the centre of the sphere (Mars) in metres, θ is the colatitude, i.e. the angle from the north pole towards the south pole and related to the latitude as $\theta = 90-$latitude, φ is the longitude, $a = 3390$ km is the mean radius of Mars, n and m are the degree and order of the spherical harmonics, $N = 62$ is the highest harmonic degree used in this model , g_{nm} and h_{hnm} are the spherical harmonics coefficients, derived by Arkani-Hamed, [2004], from MGS data.

P_n^m are the Schmidt normalised associated Legendre functions defined as

$$P_n^m(x) = \sqrt{\frac{2(n-m)!}{(n+m)!}}(1-x^2)^{m/2}\frac{\partial^m}{\partial x^m}\left[\frac{1}{2^n n!}\left[\frac{\partial^n}{\partial x^n}(x^2-1)^n\right]\right]. \tag{4.2}$$

We introduce Ampere's equation for an electrostatic case

$$\nabla \times \mathbf{B}(r,\theta,\varphi) = \mu_0 \mathbf{j} \tag{4.3}$$

and by setting the current $\mathbf{j}$ equal to zero since we assume that we do not have any currents outside the sphere (Mars) we obtain

$$\nabla \times \mathbf{B}(r,\theta,\varphi) = 0. \tag{4.4}$$

The magnetic field can now be related to the potential equation by

$$\mathbf{B}(r,\theta,\varphi) = -\nabla V \tag{4.5}$$

and written in components

$$B_r = -\frac{\partial V}{\partial r} = \sum_{n=1}^{N}(n+1)\left(\frac{a}{r}\right)^{n+2}\sum_{m=0}^{n}[(g_{nm}\cos m\varphi + h_{nm}\sin m\varphi)P_n^m(\cos\theta)], \tag{4.6}$$

$$B_\theta = -\frac{1}{r}\frac{\partial V}{\partial \theta} = -\sum_{n=1}^{N}\left(\frac{a}{r}\right)^{n+2}\sum_{m=0}^{n}\left[(g_{nm}\cos m\varphi + h_{nm}\sin m\varphi)\frac{\partial P_n^m(cos\theta)}{\partial \theta}\right], \quad (4.7)$$

where

$$\begin{cases} \frac{\partial P_n^m(\cos\theta)}{\partial\theta} = \frac{n\cos\theta P_n^m(\cos\theta) - (n+m)P_{n-1}^m(\cos\theta)}{\sqrt{1-\cos^2\theta}} & \text{n} > 1 \\ \frac{\partial P_1^0(\cos\theta)}{\partial\theta} = -\sqrt{(}2)\sin\theta & \text{n} = 1 \\ \frac{\partial P_1^1(\cos\theta)}{\partial\theta} = \cos\theta & \text{n} = 1 \end{cases} \quad (4.8)$$

and

$$B_\varphi = -\frac{1}{r\sin\theta}\frac{\partial V}{\partial \varphi} = \\ -\frac{a}{r\sin\theta}\sum_{n=1}^{N}\left(\frac{a}{r}\right)^{n+1}\sum_{m=0}^{n}[(-mg_{nm}\sin m\varphi + mh_{nm}\cos m\varphi)P_n^m(\cos\theta)]. \quad (4.9)$$

The total magnetic field strength is expressed as

$$B_{\text{tot}} = \sqrt{B_r^2 + B_\theta^2 + B_\varphi^2}. \quad (4.10)$$

4.2.1 Implementation

The three components of the magnetic field as well as the total field strength are calculated by using Matlab routines which will be briefly explained here. The main program is gomag.m, which reads in the spherical harmonics coefficients and specifies for which coordinates the magnetic field should be calculated. To calculate the magnetic field components, gomag.m first calls the function snalf.m which calculates the Schmidt normalised associated Legendre functions (SNALF:s) and their derivatives with respect to θ, for a specific θ. The routine gomag.m then calls magfield.m which actually calculates the three components of the magnetic field for a certain r, θ and φ, with associated spherical harmonic coefficients as well as the SNALF:s and their derivatives.

The three components of the magnetic field - and the total field strength - are plotted in Figure 4.3 for an altitude of 250 km with a spacing of 0.5 degrees.

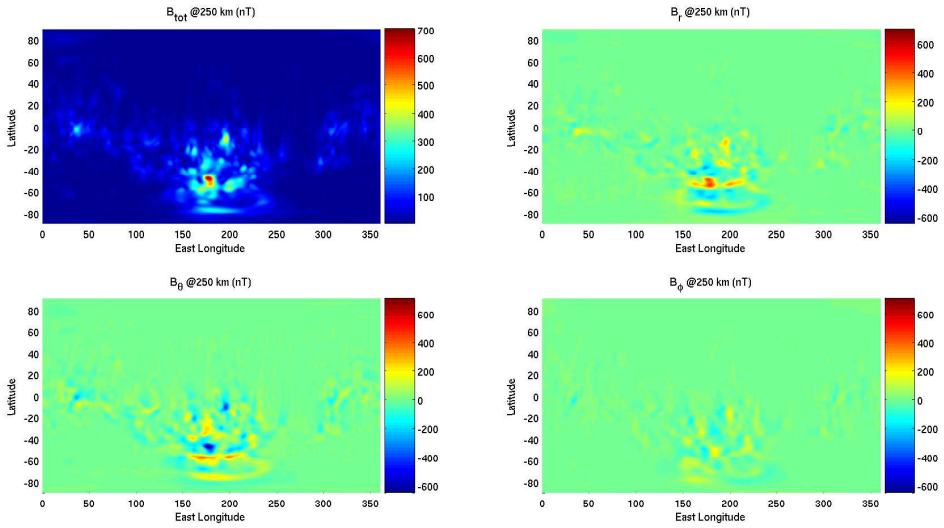

Figure 4.3: Magnetic field strength at 250 km altitude, calculated using Arkani-Hameds spherical harmonics model.

In Figure 4.4 Rosetta's path in areographical coordinates is plotted on the map of the total magnetic field strength at an altitude of 250 km. The closest approach will take place in a region where the magnetic field is very weak.

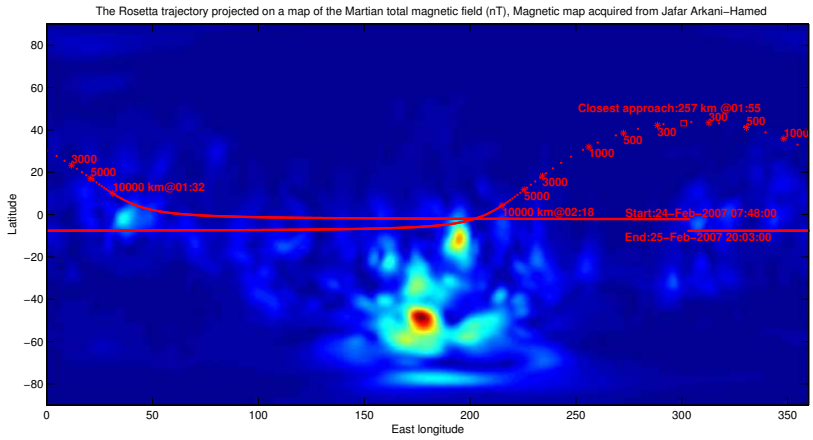

Figure 4.4: Magnetic field strength at an altitude of 250 km, with Rosetta's trajectory in areographical coordinates projected on it. Same scale on the magnetic field as in Figure 4.3.

In order to find out what values of the crustal magnetic field Rosetta can expect to encounter, each point in Rosetta's trajectory $(r, longitude, latitude)$ is cross-runned with the magnetic field model. For each set of position coordinates, all three components of the magnetic field $(B_r, B_\theta, B_\varphi)$ are calculated and time series are obtained. The results are shown in Figure 4.5.

It is also convenient to have the magnetic field as Cartesian components in the MSO reference frame, where the x-axis is directed towards the Sun. From the gomag.m program the magnetic field comes out in r, θ and φ-components in the MEO-coordinate system. The magnetic field components are therefore also transformed into Cartesian coordinates by the relations in Equations 4.11, 4.12 and 4.13,

$$B_x = B_r \sin\theta \cos\varphi + B_\theta \cos\theta \cos\varphi - B_\varphi \sin\varphi \tag{4.11}$$

$$B_y = B_r \sin\theta \sin\varphi + B_\theta \cos\theta \sin\varphi + B_\varphi \cos\varphi \tag{4.12}$$

$$B_z = B_r \cos\theta - B_\theta \sin\theta. \tag{4.13}$$

The results are shown in Figure 4.6.

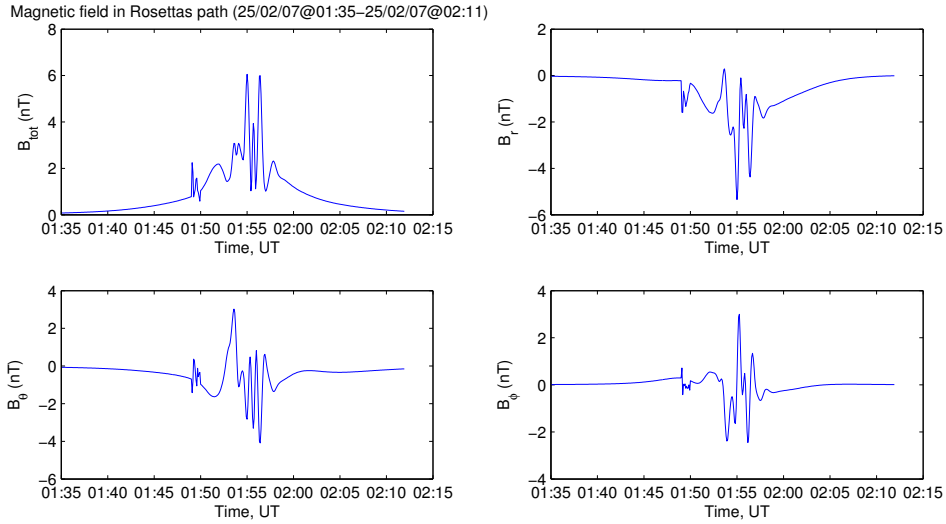

Figure 4.5: Spherical components of the magnetic field in Rosetta's path.

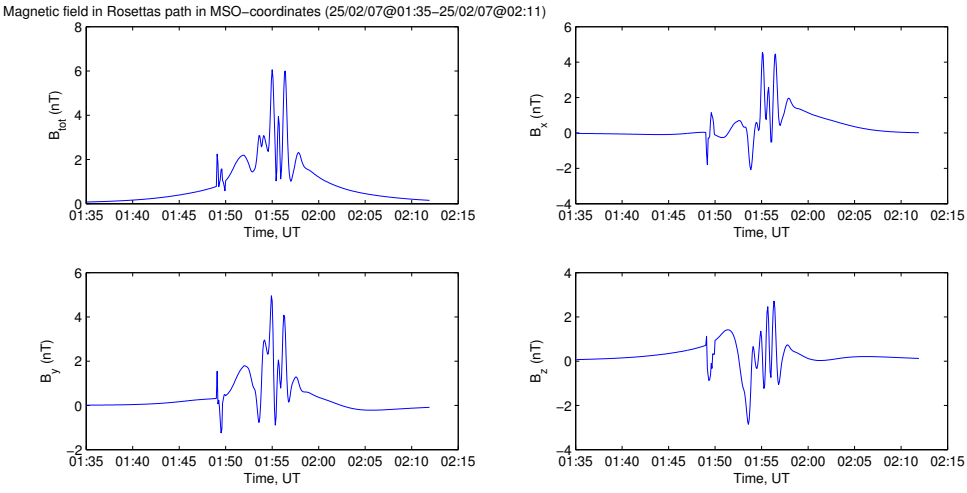

Figure 4.6: Cartesian components of the magnetic field in Rosetta's path in MSO-system. Note that the total field strength (B_{tot}) is the same as in Figure 4.5.

4.2.2 Comparing Crustal and External Magnetic Field

The external magnetic field at Mars, i.e. the interplanetary magnetic field, reaches a maximum strength of 15 nT around Mars (see Figure 3.14), while the crustal magnetic field reaches several hundreds of nT at altitudes within the ionosphere. However, the stronger crustal magnetic anomalies are local features mainly situated in the southern hemisphere while the larger part of the area of Mars have rather weak crustal magnetic anomalies. As Rosetta will have its closest approach in the nothern hemisphere (see Figure 4.4) it is most likely to encounter a region of weaker crustal field.

The crustal field changes on shorter spatial scales than the external field, making the crustal field in Rosetta's path almost oscillating, a feature clearly visible in Figures 4.5 and 4.6. In Figure 4.7 the crustal magnetic field from the model of Arkani-Hamed, [2004], is superposed on the interplanetary magnetic field from Modolo et al., [2005], in order to show that their strengths will be of the same order of magnitude but have different spatial patterns (oscillating vs. smooth). Note that this is a first order approximation of how it will look since the crustal field will disturb the ionosphere, which in turn will disturb the interplanetary magnetic field.

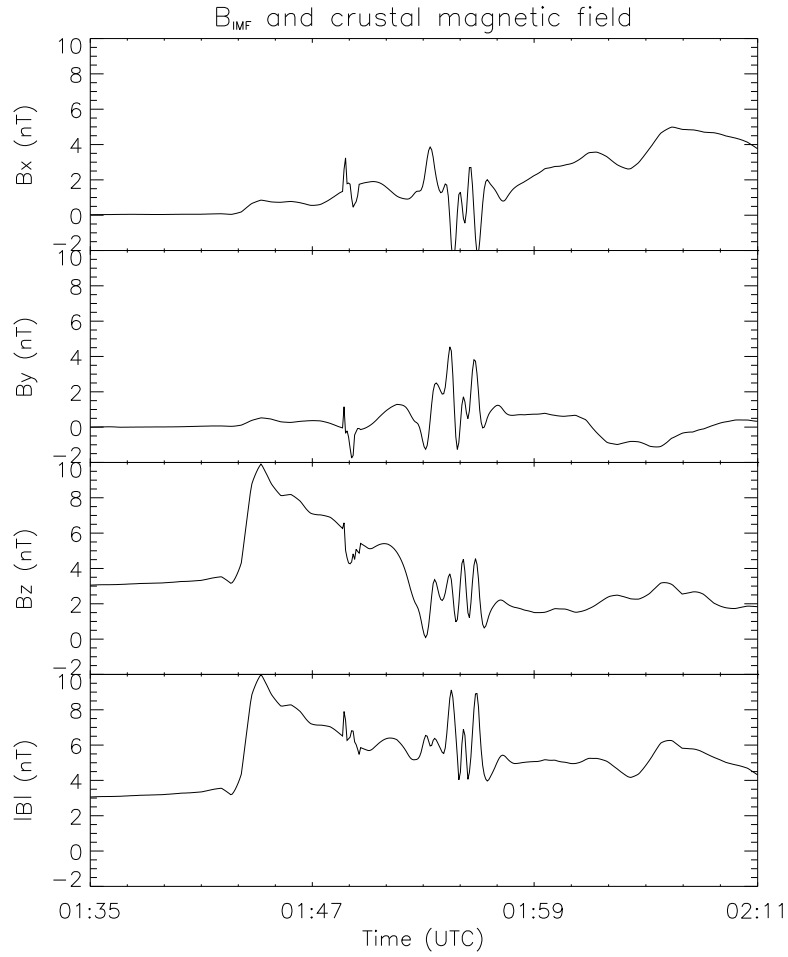

x(R_M)	−2.91	−0.95	1.07	2.91
y(R_M)	−1.92	−1.40	−0.66	0.27
z(R_M)	0.15	0.25	0.29	0.26
Alt(km)	8450.19	2401.21	1001.86	6564.09

Figure 4.7: The crustal magnetic field superposed on the interplanetary magnetic field.

4.3 Effects of the Crustal Field on the Ionosphere

When it has been shown that Martian magnetic field mainly consists of crustal anomalies, it is interesting to see how this affects the features of the ionosphere.

A planet with a major intrinsic magnetic field (like the Earth) that interacts with the solar wind produces a global magnetosphere around the planet. A small magnetic field on Mars will also produce a magnetosphere - a mini-magnetosphere. It is likely that these mini-magnetospheres on Mars, which will be mainly situated in the southern hemisphere, will extend up to an altitude of 400 km [Krymskii et al., 2003].

In the larger mini-magnetospheres, the magnetic field lines are mainly closed and hotter electrons can be trapped. The upper-most field lines can reconnect with the interplanetary magnetic field (IMF) and high-energetic solar wind particles can precipitate. "Cusps" are thereby formed and the hotter electrons are not trapped. This variation in electron density has been seen when comparing measured electron densities at different longitudes, with peak-density variation of up to 15% [Krymskii et al., 2003]. A Martian aurora have recently been discovered with the ultraviolet spectrometer, SPICAM, onboard the Mars Express spacecraft [Bertaux et al., 2005]. This Martian aurora is a highly concentrated and localised emission controlled by the magnetic field anomalies in the Martian crust.

In Withers et al., [2005], several thousand electron density profiles from the Mars Global Surveyour Radio Science experiments are studied. Their conclusions were that the ionospheric profiles changed drastically over vertical distances as short as 1–2 km. These anomalous changes mainly occurred in the southern hemisphere where the crustal mangetic fields are mainly situated. This implies that there is a correlation between the crustal magnetic anomalies and the density profile anomalies. In order to fully understand these odd features, modelling of plasma transport in the Martian magnetic field is needed. In Figure 4.8 six different electron density profiles are plotted, showing the diversity of the profiles.

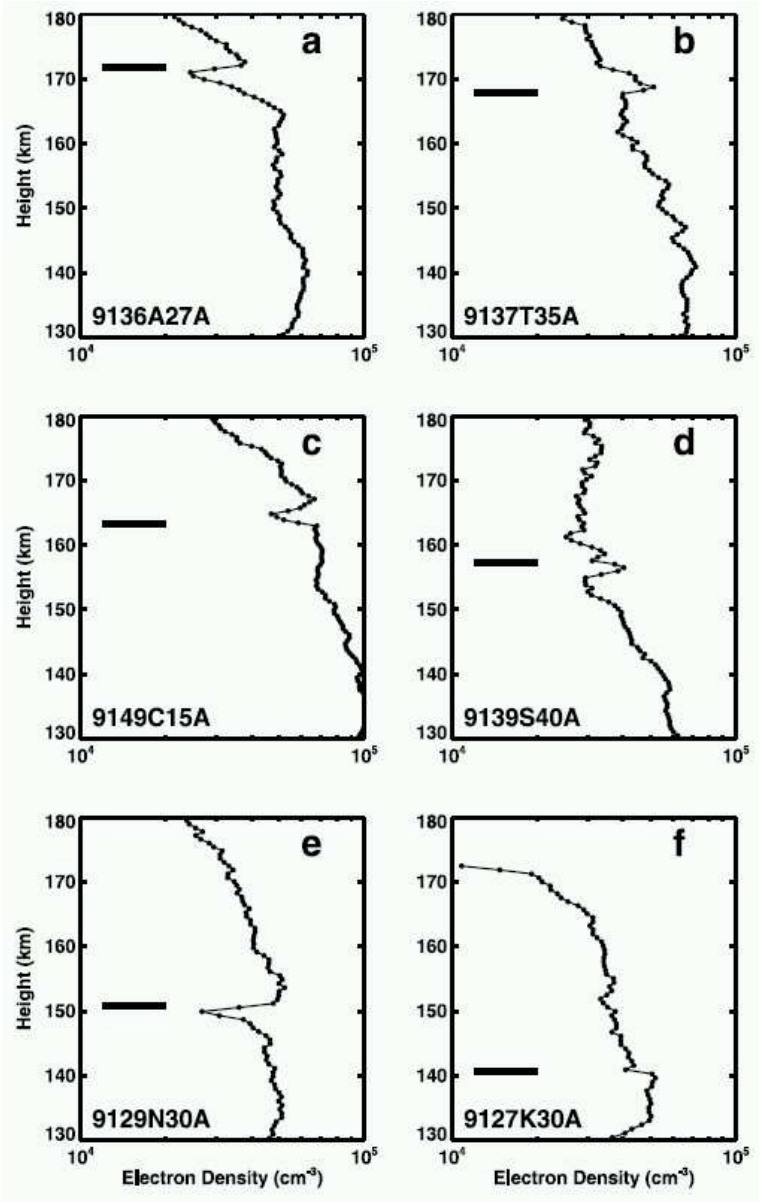

Figure 4.8: Six different electron density profiles from the ionosphere of Mars. The height of each anomalous feature is marked by a horizontal bar. Figure from Withers et al., [2005].

Chapter 5

Introduction to Langmuir Probes

Onboard Rosetta there are two Langmuir probes, which together with the associated electronics constitute the LAP instrument, designed and constructed by the Swedish Institute of Space Physics in Uppsala (IRFU). This is one of five scientific instruments forming the Rosetta Plasma Consortium (RPC), which together are responsible for the plasma measurements during this mission. This chapter will describe the principles of a dual Langmuir probe and what it is capable of measuring.

5.1 Basic Design and Function

A Langmuir probe is a conceptually very simple, but efficient scientific instrument. Basically, it consists of a metallic sphere mounted on a rod, see Figure 5.1. The spheres on the two probes on Rosetta have a radius of 2.5 cm and a rod length of 15 cm with one end fastened to a long boom. The sphere and the rod are covered by titanium nitride, which is a very suitable material in this case because of its electrical and thermal properties as well as for its robustness and chemical inertness [Boström et al., 2005].

Figure 5.1: A Langmuir probe. Figure from *www.space.irfu.se/rosetta/galleri.html*.

Some electronics are connected to the probe in order to control what is to be measured. How the electronic part is constructed is not to be explained in detail here.

As mentioned above, this probe is very efficient despite its simple construction since it can measure many different plasma parameters, depending on which mode the electronics operate in. Nevertheless, the theory underlying the probe response is not so simple.

The conducting sphere will interact with the surrounding plasma as it flies through space. The main plasma properties that it is possible to measure are the density, the temperature and the flow velocity. However, it is also possible to measure the electric field in the plasma, density fluctuations, the spacecraft's electric potential, integrated UV flux and dust impacts [Boström et al., 2005]. Explaining how this is carried out is the aim of the following sections.

5.2 Density and Electron Temperature

Basically, the probe is attached to a power supply capable of biasing it at various voltages, positive and negative, relative to the plasma. The current collected by the probe then provides information about the conditions in the plasma. By making a sweep of the bias voltage, i.e. the potential difference between the probe and the plasma $U_B = V_{\text{probe}} - V_{\text{plasma}}$, a current will arise as the plasma particles are drawn to the probe. When the bias voltage is negative, positive ions will be attracted to the probe and when the bias voltage is positive, negatively charged electrons will be attracted while positively charged ions are repelled. Depending on the value of the voltage, the current will vary and a so-called Langmuir curve will form, as can be seen in Figure 5.2. The number density and electron temperature can be derived from this curve.

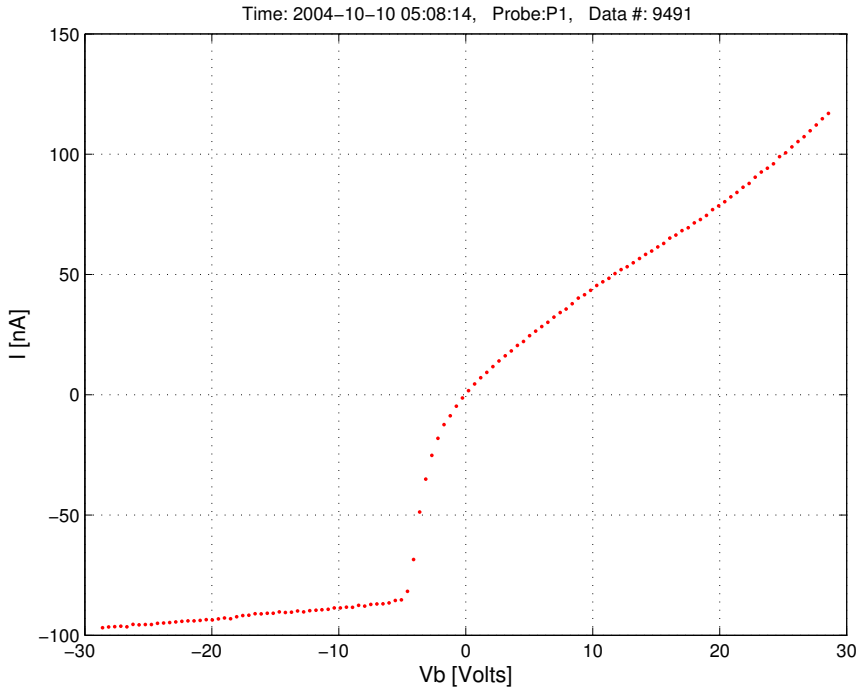

Figure 5.2: A Langmuir curve from a bias-voltage sweep by the Rosetta spacecraft's Langmuir probe No. 1. Courtesy Claes Weyde.

Electron temperature and density can be found by fitting a theoretical expression for the current-voltage relation to a measured sweep as in Figure 5.2. Alternatively, the electron temperature can be found from the nonlinear part of the curve, the sharp left knee in Figure 5.2, marking the negative of the S/C potential. Combinating with the slope of the right hand part of the curve, the electron density is obtained. The density range that is possible to measure goes from 1 cm^{-3} to 10^6 cm^{-3} and the temperature range goes from 10 meV to 10 eV.

5.3 Relative Density Changes and Plasma Flow Speed

Instead of varying the bias voltage, it can also be kept constant. By keeping the potential constant the current collected from the plasma will vary as the plasma environment changes. This makes it possible to retrieve a value of the per cent changes in density, $\delta n/n$, [Eriksson and Boström, 1995].

In order to measure the plasma flow velocity, two probes have to be used. The two probes measure the same density fluctuations, but one of them a short time before the other since they are separated in space. Comparing the two curves, they will therefore show a slight phase shift between them. Measuring the time difference between two identical peaks will give the time it took for the plasma particles to travel the (known) distance between the two probes and hence the speed of the plasma can be calculated. It is possible to measure speeds up to 10 kms^{-1}.

5.4 Electric Field and Spacecraft Potential

After having both swept the voltage and kept it constant, it is now time to work with the bias current. By keeping the current on both probes constant and by measuring the potential on each probe, one can estimate the electric field. The electric field is simply the potential difference between the probes divided by their spatial distance and can be measured up to a frequency of 8 kHz.

In this mode it is also possible to obtain an approximate value of the spacecraft potential in the range ± 32 V. This is carried out by taking the mean value of the two probe potentials.

5.5 Photoelectron Currents

A problem that can occur during the Langmuir probe measurements is the unwanted photoelectron currents. When the spacecraft is illuminated by direct sunlight, photoelectrons are emitted creating a cloud around the probe. This electron cloud gives rise to measurement errors since the photoelectrons can not be separated from the original plasma electrons.

This problem is hard to avoid since the probe can not be shielded (it has to be able to make measurements). One possible solution is to make sure that the measuring probe is in the shadow of the spacecraft. This is one of two reasons why the probes are not placed symmetrical with respect to the satellite body. The other reason is that one probe could be in wake of the other during time-of-flight measurements.

Chapter 6

Further Upcoming Events

The Rosetta mission is as mentioned a long-lasting mission. It will take an additional seven years after the Mars flyby to reach the final destination - the comet 67P/Churyumov-Gerasimenko. During these years two more Earth flybys will be conducted. The trajectories of these two flybys have been updated from Billvik, [2005], and new versions are plotted in this chapter to give a hint of what is coming.

We will also investigate the possibility for Parker spiral conjunctions between the Rosetta, Mars and the Earth. Rosetta-Mars conjunctions would give the possibility for collaboration between Rosetta science groups and other groups with spacecraft in orbit around Mars.

6.1 The Second and Third Rosetta Earth Flybys

This chapter shows 3D and 2D GSE plots of the 2nd and 3rd Earth flybys, which will take place in November 2007 and November 2009, see Figures 6.1, 6.2, 6.3 and 6.4. Note that for both flybys the approaches are from the nightside.

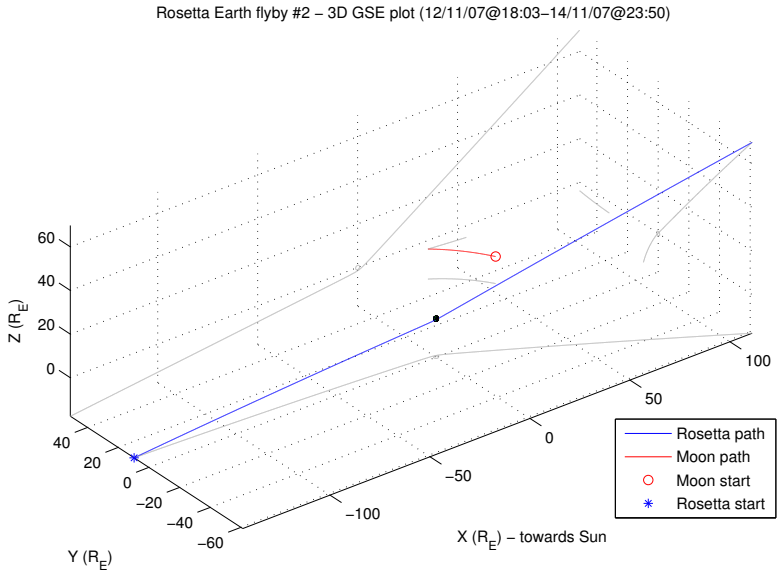

Figure 6.1: 3D view of the second Earth flyby. Rosetta will approach the Earth from the nightside.

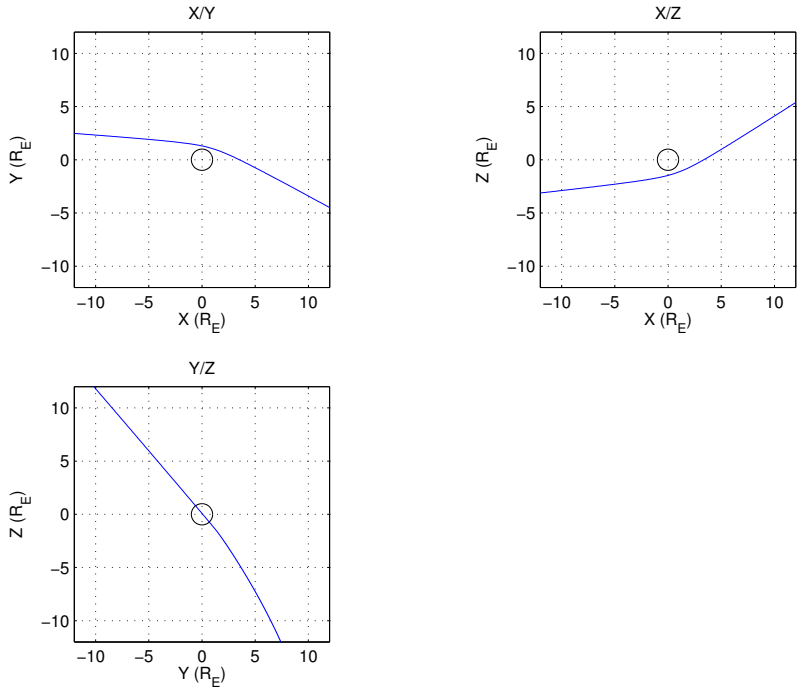

Figure 6.2: The second Earth flyby, projected on the X/Y, X/Z and Y/Z-plane.

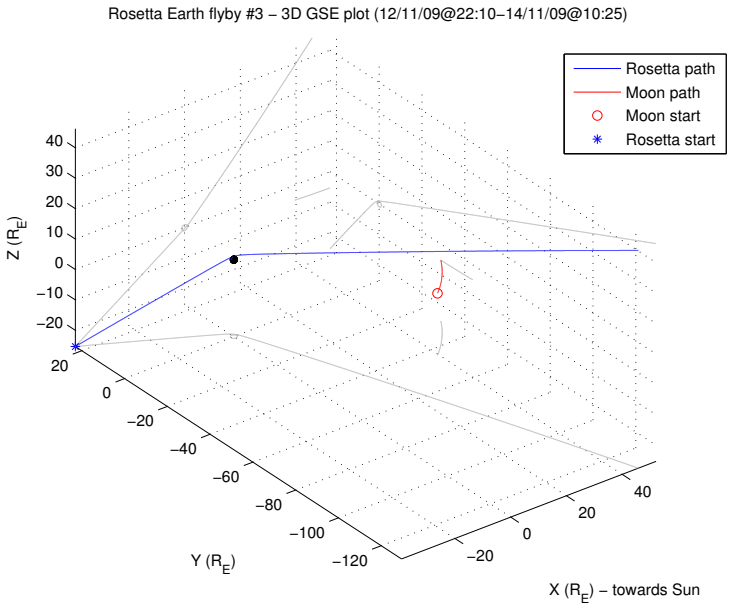

Figure 6.3: 3D view of the third Earth flyby. Rosetta will once again approach the Earth from the nightside.

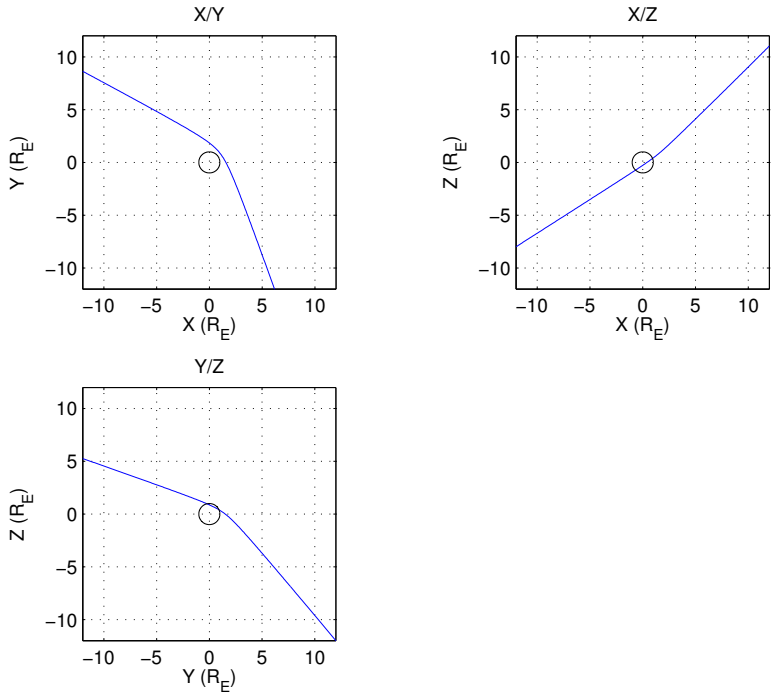

Figure 6.4: The third Earth flyby, projected on the X/Y, X/Z and Y/Z-plane..

6.2 Parker Spiral Conjunctions

A Parker spiral is a feature in the interplanetry magnetic field due to the fact that the Sun, which is the original source of the interplanetary magnetic field, rotates. The solar wind, which the interplanetary magnetic field is frozen into, moves away from the Sun at a typical speed of 300 – 700 km/s and as the Sun rotates a spiral shape will be formed of the magnetic field, see Figure 6.5.

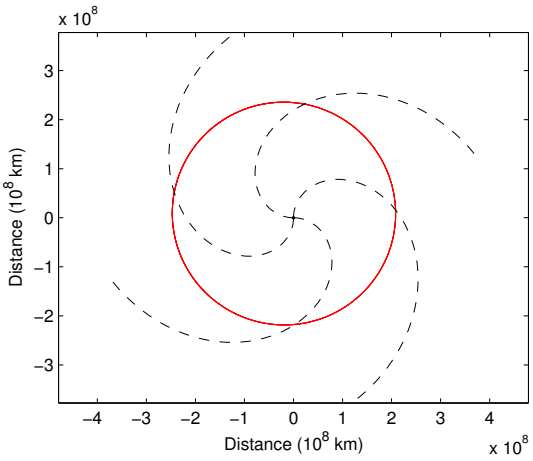

Figure 6.5: Theoretical Parker spirals (dashed line) with a solar wind speed of 400 km/s. The orbit of Mars is plotted in red.

Assuming that one region on the Sun emits a solar wind which is constant in time, the solar wind parameters along a Parker spiral field line should be constant or vary in a simple predictable way with distance from the Sun. This has for instance been used by Vennerstrom et al., [2003], for conjunctions between the Earth and Mars. Rosetta could perhaps do measurements during conjunctions between itself and Mars, and between itself and the Earth, during its long time journey. Measurements during conjunctions between the Earth and Mars could also be performed. We investigate all three possibilities in the following subsections.

The reason for investigating this is that it would be of great interest to the other satellites orbiting Mars, or the Earth, to find out the properties of the interplanetary magnetic field before it encounters the plasma environment around the planet. This would help in understanding on how the solar wind interaction with the planet works.

6.2.1 Rosetta-Mars Parker Spiral Conjunctions

Rosetta will, as mentioned, conduct its flyby of Mars in February 2007. However, Rosetta will orbit the Sun for an additional seven years after the Mars flyby, in which it might be in a Parker spiral conjunction.

To simulate such a conjunction event the Sun has been assumed to rotate with an angular velocity ω equal to one revolution in 25.38 days, or $2.87 \cdot 10^{-6}$ rad/s. Following Vennerstrom et al., [2003], and denoting the solar wind speed by v there should be a time-shift between Rosetta and Mars consisting of two terms:

$$\Delta t = \Delta t_1 + \Delta t_2 \tag{6.1}$$

$$\Delta t_1 = \frac{r_{\text{Mars}} - r_{\text{Rosetta}}}{v} \tag{6.2}$$

$$\Delta t_2 = \frac{\phi_{\text{Mars}} - \phi_{\text{Rosetta}}}{\omega} \tag{6.3}$$

where ϕ and r are the heliospheric longitude and the distance from the Sun to the respective body. This time-shift indicates how far away the two bodies are from a Parker spiral conjunction.

A perfect Parker spiral conjunction occur when the Rosetta spacecraft and Mars are aligned with a time-shift of zero, so we should look for such events. However, the timeshift is dependant on the solar wind speed which changes with time. This means that we can vary the solar wind speed from 300 – 700 km/s (an interval in which the solar wind speed in about 90 per cent of the time lies within) and then check for conjunctions. By doing so we find two conjunction events, see Table 6.1. Note that the Rosetta trajectory is not in the same plane as Mars, the Earth and also the Parker spirals which makes the model rather approximate, if the solar wind is emitted radially.

Table 6.1: Parker spiral conjunctions between Rosetta and Mars.

Conj. No.	Duration
1	07-Jan-2008 - 07-Feb-2008
2	08-Feb-2010 - 22-Feb-2010

In Figure 6.6 the two conjunction events are indicated by the thicker segments of the Mars and Rosetta orbits.

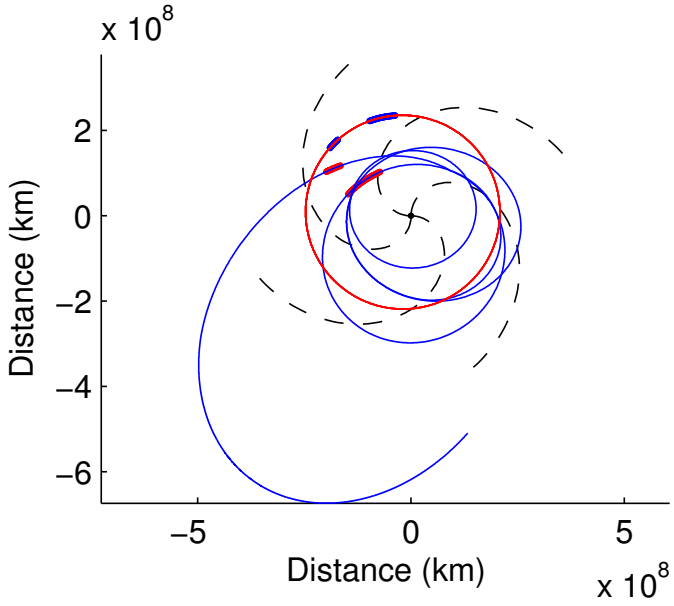

Figure 6.6: Parker spirals conjunctions are indicated as thicker segments in opposite colours (blue and red) to the trajectory curves of Mars (red) and Rosetta (blue).

6.2.2 Rosetta-Earth Parker Spiral Conjunctions

We do the same investigations on possible conjunctions between Rosetta and the Earth as we did between Rosetta and Mars an find eight such conjunctions, see Table 6.2.

Table 6.2: Parker spiral conjunctions between the Earth and Mars.

Conj. No.	Duration
1	30-Oct-2007 - 28-Dec-2007
2	19-May-2008 - 01-Aug-2008
3	26-Oct-2009 - 30-Oct-2009
4	01-Dec-2009 - 09-Dec-2009
5	18-May-2010 - 08-Nov-2010
6	13-Sep-2011 - 19-Mar-2012
7	13-Oct-2012 - 20-Mar-2013
8	14-Oct-2013 - 19-Feb-2014

6.2.3 Earth-Mars Parker Spiral Conjunctions

Finally, we investigate possible conjunctions between the Earth and Mars and find five conjunctions until 2014, see Table 6.3

Table 6.3: Parker spiral conjunctions between the Earth and Mars.

Conj. No.	Duration
1	16-Dec-2005 - 12-Feb-2006
2	03-Feb-2008 - 19-Mar-2008
3	11-Mar-2010 - 20-Mar-2010
4	13-Apr-2012 - 02-Jun-2012
5	18-May-2014 - 23-May-2014

Chapter 7

Conclusions and Outlook

The 25th of February 2007 at 01:55 UT Rosetta will have its closest approach of Mars, being the 17th successful spacecraft in order to ever visit the planet. The path of the spacecraft lies well within the ionosphere and the plasma environment of the planet. It is therefore an opportunity for plasma investigations and planetary exploration. The Swedish Institute of Space Physics in Uppsala has contributed to the payload onboard with one instrument incorporated in the Rosetta Plasma Consortium. Two Langmuir probes used for plasma measurements will investigate the environment around Mars.

The trajectory of Rosetta has been determined by further development of Matlab routines for reading in trajectory data and making coordinate transformations. By plotting the trajectory we find that Rosetta will approach Mars from the dayside and swing by to the nightside of the planet, proceeding out through the magnetic tail. After about two hours within the plasma environment Rosetta will have passed all major plasma boundaries and regions, all detectable by the Langmuir probes. We conclude that a 24 minute eclipse will occur as Rosetta is shadowed by Mars. There will also be an additional four spacecraft at Mars during the flyby, which gives the opportunity for unique multi-spacecraft measurements.

By using an existing 3D simulation of the Martian plasma environment we obtain time series of expected plasma density, temperature, flow velocity, drift kinetic energy and effective ion mass in Rosetta's path. This will help in setting the onboard instruments in right modes and also help to interpret the measurements. For instance, the simulation gives a maximum value of $1 \cdot 10^3$ cm^{-3} of the plasma density. However, this is an uncertain value since other density profiles from literature indicate a maximum value twenty times higher. Literature studies indicate that the ion and electron temperatures at an altitude of 250 km are on the order of 2000 K and 3000 K (or 0.17 eV 0.26 eV), respectively.

We implement an existing model of the crustal magnetic field of Mars which is the only intrinsic magnetic field of importance. This relatively strong field is remnant from an earlier epoch when a global magnetic field have existed. Today, the crustal magnetic

field is mainly situated in the southern hemisphere. We have found that since Rosetta will have the closest approach on the northern hemisphere where the magnetic anomalies are weaker, the magnetometers onboard will measure both crustal magnetic field and interplanetary magnetic field on the same order of magnitude, i.e. about 10 nT. The crustal field might be possible to discern by its high frequency oscillations.

Finally, we investigate some further upcoming events. We look at the trajectories of the second and third Earth flybys in November 2007 and November 2009 and conclude that Rosetta will approach the Earth from the nightside and follow the magnetic tail all the way in to the closest approach for both flybys.

We also model possible Parker spiral conjunctions between Rosetta and Mars. Two such conjunctions were found, one in early 2008 and one in February 2010. We model conjunctions between the Earth and Mars as well and also between Rosetta and the Earth and find five and eight conjunctions, respectively.

In the near future, the attitude of the spacecraft will be determined and the scientific instruments onboard Rosetta will need be set to work in the right measuring mode during the flyby. In one year from the writing of this report, measurements from another planet will be conducted and data sent back to the Earth. Hopefully, the measurements will be successful and the analysis can take place, showing the features of the plasma environment at Mars.

Acknowledgements

First of all I would like to thank my supervisor Anders Eriksson for his dedication and never-ending interest during this thesis work, for always being helpful and encouraging - a splendid supervisor.

I owe Ronan Modolo my deepest and most humble gratitude for providing me with his model of the Martian plasma environment. He dedicated many hours of his time helping me with the simulations as well as proofreading the final report. Jafar Arkani-Hamed provided the crustal magnetic field model, Pär-Ola Nilsson helped in finding trajectory data files and Mats André gave useful comments on the report - I thank them all.

I would also like to give a warm thanks to Karin Ågren for always being there, as a co-worker and as a partner. For the wonderful time at IRFU I thank the entire staff, especially my fellow thesis workers for many joyful lunches and coffee breaks and among them Oscar Stål, for interesting conversations as well as for giving many useful comments on the report.

Bibliography

[Acuña et al., 1999] Acuña, M. H., Connerney, J. E. P., Ness, N. F., Lin, R. P., Mitchell, D., Carlson, C. W., McFadden, J., Anderson, K. A., Reme, H., Mazelle, C., Vignes, D., Wasilewski, P., and Cloutier, P. (1999). Global Distribution of Crustal Magnetization Discovered by the Mars Global Surveyor MAG/ER Experiment. *Science*, 284:790.

[Acuña et al., 1998] Acuña, M. H., Connerney, J. E. P., Wasilewski, P., Lin, R. P., Anderson, K. A., Carlson, C. W., McFadden, J., Curtis, D. W., Mitchell, D., Reme, H., Mazelle, C., Sauvaud, J. A., D'Uston, C., Cros, A., Medale, J. L., Bauer, S. J., Cloutier, P., Mayhew, M., Winterhalter, D., and Ness, N. F. (1998). Magnetic Field and Plasma Observations at Mars: Initial Results of the Mars Global Surveyor Mission. *Science*, 279:1676.

[Arkani-Hamed, 2004] Arkani-Hamed, J. (2004). A coherent model of the crustal magnetic field of Mars. *Journal of Geophysical Research (Planets)*, 109(E18):9005.

[Bertaux et al., 2005] Bertaux, J.-L., Leblanc, F., Witasse, O., Quemerais, E., Lilensten, J., Stern, S. A., Sandel, B., and Korablev, O. (2005). Discovery of an aurora on Mars. *Nature*, 435:790–794.

[Bertucci et al., 2003] Bertucci, C., Mazelle, C., Crider, D. H., Vignes, D., Acuña, M. H., Mitchell, D. L., Lin, R. P., Connerney, J. E. P., Rème, H., Cloutier, P. A., Ness, N. F., and Winterhalter, D. (2003). Magnetic field draping enhancement at the Martian magnetic pileup boundary from Mars global surveyor observations. *Geophysical Research Letters*, 30:71–1.

[Billvik, 2005] Billvik, M. (2005). The First Rosetta Earth Flyby. Master's thesis, Uppsala University.

[Boström et al., 2005] Boström, R., Eriksson, A. I., Åhlen, L., Blomberg, L., Gustafsson, G., Holback, B., Holmgren, G., Holtet, J., Jansson, S. E., Lindqvist, P. A., Lybekk, B., Mälkki, A., Riihelä, P., Stasiewicz, K., and Wahlund, J. E. a. (2005). LAP-RPC: The Rosetta Dual Langmuir Probe of the Rosetta Plasma Consortium,. ESA Scientific Report in press.

[Cain et al., 2003] Cain, J. C., Ferguson, B. B., and Mozzoni, D. (2003). An n = 90 internal potential function of the Martian crustal magnetic field. *Journal of Geophysical Research (Planets)*, 108(E2):2–1.

[Crider et al., 2003] Crider, D. H., Vignes, D., Krymskii, A. M., Breus, T. K., Ness, N. F., Mitchell, D. L., Slavin, J. A., and Acuña, M. H. (2003). A proxy for determining solar wind dynamic pressure at Mars using Mars Global Surveyor data. *Journal of Geophysical Research (Space Physics)*, 108(A12):21–1.

[Danby, 1988] Danby, J. M. A. (1988). *Fundamentals of Celestial Mechanics*. William-Bell, Inc., 2nd edition.

[Duxbury et al., 2001] Duxbury, T. C., Kirk, R. L., Archinal, B. A., and Neumann, G. A. (2001). Mars Geodesy/Cartography Working Group Recommendations on Mars Cartographic Constants and Coordinate Systems. In *ISPRS WG IV/9: Extraterrestrial Mapping Workshop - Planetary Mapping Workshop, virtual workshop*.

[Eriksson and Boström, 1995] Eriksson, A. I. and Boström, R. (1995). Measurements of Plasma Density Fluctuations and Electric Wave Fields Using Spherical Electrostatic Probes. Technical report, Swedish Institute od Space Physics.

[Fox et al., 1996] Fox, J. L., Zhou, P., and Bougher, S. W. (1996). The Martian thermosphere/ionosphere at high and low solar activities. *Advances in Space Research*, 17:203–218.

[Grard et al., 1991] Grard, R., Nairn, C., Pedersen, A., Klimov, S., Savin, S., Skalsky, A., and Trotignon, J. G. (1991). Plasma and waves around Mars. *Planetary and Space Science*, 39:89–93.

[Hapgood, 1997] Hapgood, M. A. (1997). Space Physics coordinate transformations: a user guide. *Planetary and Space Science*, 45:1047.

[JPL's Horizons System, 2005] JPL's Horizons System (2005). Internet page. http://ssd.jpl.nasa.gov/horizons.html.

[Krymskii et al., 2003] Krymskii, A. M., Breus, T. K., Ness, N. F., Hinson, D. P., and Bojkov, D. I. (2003). Effect of crustal magnetic fields on the near terminator ionosphere at Mars: Comparison of in situ magnetic field measurements with the data of radio science experiments on board Mars Global Surveyor. *Journal of Geophysical Research (Space Physics)*, 108(A12):5–1.

[Langlais et al., 2004] Langlais, B., Purucker, M. E., and Mandea, M. (2004). Crustal magnetic field of Mars. *Journal of Geophysical Research (Planets)*, 109(E18):2008.

[Liu et al., 2001] Liu, Y., Nagy, A. F., Gombosi, T. I., Dezeeuw, D. L., and Powell, K. G. (2001). The solar wind interaction with Mars: results of three-dimensional three-species MHD studies. *Advances in Space Research*, 27:1837–1846.

[Lundin and Barabash, 2004] Lundin, R. and Barabash, S. (2004). Evolution of the Martian atmosphere and hydrosphere: Solar wind erosion studied by ASPERA-3 on Mars Express. *Planetary and Space Science*, 52:1059–1071.

[Martinis et al., 2003] Martinis, C. R., Wilson, J. K., and Mendillo, M. J. (2003). Modeling day-to-day ionospheric variability on Mars. *Journal of Geophysical Research (Space Physics)*, 108:8–1.

[Modolo et al., 2005] Modolo, R., Chanteur, G. M., Dubinin, E., and Matthews, A. P. (2005). Influence of the solar EUV flux on the Martian plasma environment. *Annales Geophysicae*, 23:433–444.

[Moffat, 2005] Moffat, T. (2005). *The UCL Martian Thermosphere and Ionosphere Global Circulation Modal: Development and Validation.* PhD thesis, Department of Physics and Astronomy, University College London.

[Nagy et al., 2004] Nagy, A. F., Winterhalter, D., Sauer, K., Cravens, T. E., Brecht, S., Mazelle, C., Crider, D., Kallio, E., Zakharov, A., Dubinin, E., Verigin, M., Kotova, G., Axford, W. I., Bertucci, C., and Trotignon, J. G. (2004). The plasma Environment of Mars. *Space Science Reviews*, 111:33–114.

[Nordling and Österman, 1999] Nordling, C. and Österman, J. (1999). *Physics Handbook for Science and Engineering.* Studentlitteratur, 6th edition.

[NSSDC Master catalog, 2005] NSSDC Master catalog (2005). Internet page. http://nssdc.gsfc.nasa.gov/.

[NSSDC Master catalog, Mars, 2005] NSSDC Master catalog, Mars (2005). Internet page. http://nssdc.gsfc.nasa.gov/planetary/factsheet/marsfact.html.

[Øieroset et al., 2004] Øieroset, M., Mitchell, D. L., Phan, T. D., Lin, R. P., Crider, D. H., and Acuña, M. H. (2004). The Magnetic Field Pile-up and Density Depletion in the Martian Magnetosheath: A Comparison with the Plasma Depletion Layer Upstream of the Earth's Magnetopause. *Space Science Reviews*, 111:185–202.

[Purucker et al., 2000] Purucker, M., Ravat, D., Frey, H., Voorhies, C., Sabaka, T., and Acuña, M. (2000). An altitude-normalized magnetic map of Mars and its interpretation. *Geophysical Research Letters*, 27:2449–2452.

[Råde and Westergren, 1998] Råde, L. and Westergren, B. (1998). *Mathematics Handbook for Science and Engineering.* Studentlitteratur, 4th edition.

[The Planetary Society, 2005] The Planetary Society (2005). Internet page. http://www.planetary.org/learn/missions/marsmissions.html.

[Trotignon et al., 2000] Trotignon, J. G., Parrot, M., Cerisier, J. C., Menvielle, M., Axford, W. I., Paëtzold, M., Warnant, R., and Wernik, A. W. (2000). The plasma environment of Mars: from the shocked solar wind down to the ionosphere. *Planetary and Space Science*, 48:1181–1191.

[Trotognon, 2002] Trotognon, J. G. (2002). *Rosetta/RPC Flight Operations, The Mars fly-by - Some Introductory Elements*.

[Vennerstrom et al., 2003] Vennerstrom, S., Olsen, N., Purucker, M., Acuña, M. H., and Cain, J. C. (2003). The magnetic field in the pile-up region at Mars, and its variation with the solar wind. *Geophysical Research Letters*, 30:22–1.

[Withers et al., 2005] Withers, P., Mendillo, M., Rishbeth, H., Hinson, D., and Arkani-Hamed, J. (2005). Ionospheric characteristics above martian crustal magnetic anomalies. *AAS/Division for Planetary Sciences Meeting Abstracts*, 37:1–4.

Appendix A

Coordinate Transformations

A.1 Rotation of Axes

If a right-handed rectangular system is rotated positively with the angle θ around the x-axis, then the new coordinates (x', y', z') are then related to the old ones (x, y, z) by

$$\begin{bmatrix} x' \\ y' \\ z' \end{bmatrix} = \begin{bmatrix} 1 & 0 & 0 \\ 0 & \cos\theta & \sin\theta \\ 0 & -\sin\theta & \cos\theta \end{bmatrix} \begin{bmatrix} x \\ y \\ z \end{bmatrix} = P(\theta) \begin{bmatrix} x \\ y \\ z \end{bmatrix}. \tag{A.1}$$

In the same way, a rotation around the y-axis is given by

$$\begin{bmatrix} x' \\ y' \\ z' \end{bmatrix} = \begin{bmatrix} \cos\theta & 0 & -\sin\theta \\ 0 & 1 & 0 \\ \sin\theta & 0 & \cos\theta \end{bmatrix} \begin{bmatrix} x \\ y \\ z \end{bmatrix} = Q(\theta) \begin{bmatrix} x \\ y \\ z \end{bmatrix}, \tag{A.2}$$

and a rotation around the z-axis is given by

$$\begin{bmatrix} x' \\ y' \\ z' \end{bmatrix} = \begin{bmatrix} \cos\theta & \sin\theta & 0 \\ -\sin\theta & \cos\theta & 0 \\ 0 & 0 & 1 \end{bmatrix} \begin{bmatrix} x \\ y \\ z \end{bmatrix} = R(\theta) \begin{bmatrix} x \\ y \\ z \end{bmatrix}. \tag{A.3}$$

To go from (x', y', z') to (x, y, z) the transpose of P, Q and R, called P', Q' and R', are used [Danby, 1988].

A.2 Transformation from MEI to MRX

A transformation matrix from the MEI coordinate system to the MRX system is derived below. The MEI system has the x-axis pointing towards the Earth's vernal equinox (first point of Aries) and the z-axis normal to the Earth's equator while the MRX system has

the x-axis pointing towards the vernal equinox of Mars and the z-axis normal to the equator equator of Mars. Both systems are centred in Mars.

The definitions of the new basis vectors $(\hat{x}_{\mathrm{MRX}}, \hat{y}_{\mathrm{MRX}}, \hat{z}_{\mathrm{MRX}})$ are

$$\begin{aligned} \hat{x}_{\mathrm{MRX}} &= \hat{S}_{\mathrm{Earth}} \times \hat{L}_{\mathrm{Mars}} \\ \hat{y}_{\mathrm{MRX}} &= \hat{z}_{\mathrm{MRX}} \times \hat{x}_{\mathrm{MRX}}\,, \\ \hat{z}_{\mathrm{MRX}} &= \hat{S}_{\mathrm{Earth}} \end{aligned} \tag{A.4}$$

where $\hat{S}_{\mathrm{Earth}}$ is the spin axis of the Earth and $\hat{L}_{\mathrm{Mars}}$ is the orbital momentum vector of Mars, i.e. the vector normal to Mars' orbital plane.

The Earth spin axis can be expressed in the old axes $(\hat{x}_{\mathrm{MEI}}, \hat{y}_{\mathrm{MEI}}, \hat{z}_{\mathrm{MEI}})$ as

$$\hat{S}_{\mathrm{Earth}} = \hat{x}_{\mathrm{MEI}} \cos D_s \cos R_s + \hat{y}_{\mathrm{MEI}} \cos D_s \sin R_s + \hat{z}_{\mathrm{MEI}} \sin D_s, \tag{A.5}$$

where D_s is the declination of the north pole of Mars, i.e. the angle from the Earth equator to the north pole of Mars, and R_s is the right ascension of the north pole of Mars, i.e. the angle from the Earth vernal equinox to the north pole of Mars.

The orbital momentum vector can be expressed in the MEI system as

$$\begin{aligned} \hat{L}_{\mathrm{Mars}} = -\hat{x}_{\mathrm{MEI}} \cos A_o \sin D_o + \hat{y}_{\mathrm{MEI}} (\sin D_o \sin A_o \cos\varphi + \cos D_o \sin\varphi) + \\ \hat{z}_{\mathrm{MEI}} (-\sin D_o \sin A_o \sin\varphi + \cos D_o \cos\varphi), \end{aligned} \tag{A.6}$$

where D_o is the inclination of Mars orbit with respect to the ecliptic, A_o is the longitude of the ascending node for Mars and φ is the axial obliquity of Earth, i.e. the tilt of the spin axis with respect to the ecliptic.

Calculating the cross products above and normalizing the basis vectors $(\hat{x}_{\mathrm{MRX}}, \hat{y}_{\mathrm{MRX}}, \hat{z}_{\mathrm{MRX}})$, the transformation from MEI to MRX can be written as

$$\begin{bmatrix} x_{\mathrm{MRX}} \\ y_{\mathrm{MRX}} \\ z_{\mathrm{MRX}} \end{bmatrix} = \begin{bmatrix} [\hat{x}_{\mathrm{MRX}}] \\ [\hat{y}_{\mathrm{MRX}}] \\ [\hat{z}_{\mathrm{MRX}}] \end{bmatrix} \begin{bmatrix} x_{\mathrm{MEI}} \\ y_{\mathrm{MEI}} \\ z_{\mathrm{MEI}} \end{bmatrix}, \tag{A.7}$$

where $[\hat{x}_{\mathrm{MRX}}]$ means the row vector with the normalized basis vector components.

Appendix B

Mars Facts

B.1 Mars Mean Orbital Elements

Table B.1: A list of the Mars mean orbital elements of epoch J2000 [NSSDC Master catalog, Mars, 2005].

Semimajor axis	1.52366231 AU
Orbital eccentricity	0.09341233
Orbital inclination	1.85061°
Longitude if ascending node	49.57854°
Longitude of perihelion	336.04084°
Mean longitude	355.45332°

B.2 Orbital Parameters

Table B.2: Orbital parmeters of Mars [NSSDC Master catalog, Mars, 2005].

Siderial orbit period	686.980 days
Tropical orbit period	686.973 days
Perihelion	$206.62 \cdot 10^6$km
Aphelion	$249.23 \cdot 10^6$km
Synodic period	779.94 days
Mean orbital velocity	24.13 km/s
Max. orbital velocity	26.50 km/s
Min. orbital velocity	21.97 km/s
Sidereal rotation period	24.6229 hours
Length of day	24.6597 hours
Obliquity to orbit	25.19°

B.3 North Pole of Rotation

Right Ascension: 317.681 - 0.108T

Declination : 52.886 - 0.061T

Reference Date : 12:00 UT 1 Jan 2000 (JD 2451545.0)

T = Julian centuries from reference date [NSSDC Master catalog, Mars, 2005]

B.4 Bulk parameters

Table B.3: Some bulk parameters of Mars [NSSDC Master catalog, Mars, 2005].

Mass	$0.64185 \cdot 10^{24}$kg
Volume	$16.318 \cdot 10^{10}$km^3
Equatorial radius	3397 km
Polar radius	3375 km
Volumetric mean radius	3390 km
Core radius	1700 km
Ellipticity (Flattening)	0.00648
Mean density	3933 kg/m^3
Surface gravity	3.71 m/s^2
Escape velocity	5.03 km/s
GM	$0.04283 \cdot 10^6$km^3/s^2
Bond albedo	0.250
Visual geometric albedo	0.150
Visual magnitude V(1,0)	-1.52
Solar irradiance	589.2 W/m^2
Black-body temperature	210.1 K
Topographic range	30 km
Moment of inertia (I/MR^2)	0.366
J_2	$1960.45 \cdot 10^{-6}$
Number of natural satellites	2 (Phobos and Deimos)

Appendix C

Matlab Routines

Matlab routines that have been written during this work can be found on the webpage:

`http://www.space.irfu.se/exjobb/2005_niklas_edberg/index.html`

The site includes code for reading in trajectory data, transforming between several coordinate systems and plotting the results in numerous ways.